UNIVERSIDAD DE INVESTIGACIÓN DE TECNOLOGÍA EXPERIMENTAL YACHAY

Escuela de Ciencias Físicas y Nanotecnología

TÍTULO: Tight binding description of the electron-phonon and spin-phonon interactions in electron transfer in DNA

Trabajo de integración curricular presentado como requisito para la obtención del título de Ingeniero en Nanotecnología

Autor:
Steven Andrés Feijoo Valarezo

Tutor:
Ph.D Mayra Peralta

Co-Tutor:
Ph.D Ernesto Medina

Urcuquí, Agosto 2022

Urcuquí, 28 de julio de 2022

SECRETARÍA GENERAL
ESCUELA DE CIENCIAS FÍSICAS Y NANOTECNOLOGÍA
CARRERA DE NANOTECNOLOGÍA
ACTA DE DEFENSA No. UITEY-PHY-2022-00013-AD

En la ciudad de San Miguel de Urcuquí, Provincia de Imbabura, a los 28 días del mes de julio de 2022, a las 14:00 horas, en el Aula S_CAN de la Universidad de Investigación de Tecnología Experimental Yachay y ante el Tribunal Calificador, integrado por los docentes:

Presidente Tribunal de Defensa	Dr. PINTO ESPARZA, HENRY PAUL , Ph.D.
Miembro No Tutor	Dr. COSENZA MICELI, MARIO GIUSEPPE , Ph.D.
Tutor	Dra. PERALTA ARCIA, MAYRA ALEJANDRA DE JESUS , Ph.D.

Se presenta el(la) señor(ita) estudiante **FEIJOO VALAREZO, STEVEN ANDRES**, con cédula de identidad No. **0704743491**, de la **ESCUELA DE CIENCIAS FÍSICAS Y NANOTECNOLOGÍA**, de la Carrera de **NANOTECNOLOGÍA**, aprobada por el Consejo de Educación Superior (CES), mediante Resolución **RPC-SO-13-No.156-2015**, con el objeto de rendir la sustentación de su trabajo de titulación denominado: **TIGHT BINDING DESCRIPTION OF THE ELECTRON-PHONON AND SPIN-PHONON INTERACTIONS IN ELECTRON TRANSFER IN DNA.**, previa a la obtención del título de **INGENIERO/A EN NANOTECNOLOGÍA**.

El citado trabajo de titulación, fue debidamente aprobado por el(los) docente(s):

Tutor	Dra. PERALTA ARCIA, MAYRA ALEJANDRA DE JESUS , Ph.D.
Co - Tutor	Dr. MEDINA DAGGER, ERNESTO ANTONIO , Ph.D.

Y recibió las observaciones de los otros miembros del Tribunal Calificador, las mismas que han sido incorporadas por el(la) estudiante.

Previamente cumplidos los requisitos legales y reglamentarios, el trabajo de titulación fue sustentado por el(la) estudiante y examinado por los miembros del Tribunal Calificador. Escuchada la sustentación del trabajo de titulación, que integró la exposición de el(la) estudiante sobre el contenido de la misma y las preguntas formuladas por los miembros del Tribunal, se califica la sustentación del trabajo de titulación con las siguientes calificaciones:

Tipo	Docente	Calificación
Miembro Tribunal De Defensa	Dr. COSENZA MICELI, MARIO GIUSEPPE , Ph.D.	10,0
Presidente Tribunal De Defensa	Dr. PINTO ESPARZA, HENRY PAUL , Ph.D.	9,4
Tutor	Dra. PERALTA ARCIA, MAYRA ALEJANDRA DE JESUS , Ph.D.	9,5

Lo que da un promedio de: **9.6 (Nueve punto Seis)**, sobre 10 (diez), equivalente a: **APROBADO**

Para constancia de lo actuado, firman los miembros del Tribunal Calificador, el/la estudiante y el/la secretario ad-hoc.

FEIJOO VALAREZO, STEVEN ANDRES
Estudiante

Dr. PINTO ESPARZA, HENRY PAUL , Ph.D.
Presidente Tribunal de Defensa

Dra. PERALTA ARCIA, MAYRA ALEJANDRA DE JESUS , Ph.D.
Tutor

Dr. COSENZA MICELI, MARIO GIUSEPPE , Ph.D.
Miembro No Tutor

CIFUENTES TAFUR, EVELYN CAROLINA
Secretario Ad-hoc

AUTORÍA

Yo, **STEVEN ANDRÉS FEIJOO VALAREZO**, con cédula de identidad 0704743491, declaro que las ideas, juicios, valoraciones, interpretaciones, consultas bibliográficas, definiciones y conceptualizaciones expuestas en el presente trabajo; así cómo, los procedimientos y herramientas utilizadas en la investigación, son de absoluta responsabilidad de el/la autora (a) del trabajo de integración curricular. Así mismo, me acojo a los reglamentos internos de la Universidad de Investigación de Tecnología Experimental Yachay.

Urcuquí, Agosto 2022.

STEVEN ANDRES FEIJOO VALAREZO

Firmado digitalmente por STEVEN ANDRES FEIJOO VALAREZO
Fecha: 2022.08.22 17:41:57 -05'00'

Steven Andrés Feijoo Valarezo
CI: 0704743491

AUTORIZACIÓN DE PUBLICACIÓN

Yo, **STEVEN ANDRÉS FEIJOO VALAREZO,** con cédula de identidad 0704743491, cedo a la Universidad de Investigación de Tecnología Experimental Yachay, los derechos de publicación de la presente obra, sin que deba haber un reconocimiento económico por este concepto. Declaro además que el texto del presente trabajo de titulación no podrá ser cedido a ninguna empresa editorial para su publicación u otros fines, sin contar previamente con la autorización escrita de la Universidad.

Asimismo, autorizo a la Universidad que realice la digitalización y publicación de este trabajo de integración curricular en el repositorio virtual, de conformidad a lo dispuesto en el Art. 144 de la Ley Orgánica de Educación Superior

Urcuquí, Agosto 2022.

STEVEN ANDRES FEIJOO VALAREZO

Firmado digitalmente por STEVEN ANDRES FEIJOO VALAREZO
Fecha: 2022.08.22 17:42:26 -05'00'

Steven Andrés Feijoo Valarezo
CI: 0704743491

Dedication

This work is dedicated to my family who have supported me through my studies by giving me everything that I needed, and made this possible. Also, this is dedicated to the friends I made along the way that inspired me to be better in many ways by teaching me numerous lessons. To the colleagues before me that improved my studies; and the ones after me. Finally, to the reader, the one that allows scientist to exist.

Acknowledgements

I want to thank all my professors for teaching me, not only the required information but also the things that will improve my career and future. Thanks to my tutor Ph.D Mayra Peralta and co-tutor Ph.D Ernedto Medina for guiding me through the process of investigation, for teaching me how to research, and inspiring me to achieve excellency.

Resumen

La estructura única del ADN está ligada a la amplia gama de propiedades interesantes que ha mostrado esta molécula. Últimamente, las propiedades electrónicas de esta molécula llamaron la atención en el campo de la espintrónica, en concreto, debido a la capacidad de actuar como filtro de espín. Sin embargo, el mecanismo que controla este comportamiento aún no se ha aclarado; además en experimentos sobre la conducción del ADN se observó comportamiento de aislante, en otros se observaban comportamiento de semiconductor, conductor o superconductor. Para continuar con esta línea de investigación y descubrir cómo hacer nuevos dispositivos usando ADN, este trabajo trata de describir su transferencia de electrones en base a los orbitales pi en la forma B de esta molécula, considerando los efectos de fonón y espín; que están presentes en condiciones fisiológicas, donde las aplicaciones son más importantes. Usando la aproximación de dos centros, la función envolvente, la función de suavizado y la aproximación de enlace fuerte, se desarrollaron dos modelos para estudiar la transferencia electrónica en el ADN. Se encontró que los fonones tienen relevancia tanto en la transferencia intra-hélice como inter-hélice; mientras que la interacción espín-fonón se encuentra solo en intra-hélice con cambio de espín. Los fonones ópticos se acoplan a los electrones en primer orden mientras que los acústicos solo se acoplan en segundo orden, por lo que los modos ópticos son mucho más relevantes. El acoplamiento intra-hélice sin cambio de espín consiste en un término cinético de segundo orden, por lo que las interacciones de fonón y espín no afectan a este acoplamiento. En conclusión, el modelo fue capaz de hacer predicciones describiendo cualitativamente la persistencia de la coherencia implícita en los experimentos.

Palabras clave: Aproximación de enlace fuerte, ácido desoxirribonucleico, transferencia electronica, electrón-fonón, espín-fonón.

Abstract

The unique structure of DNA is bound to the wide range of interesting properties this molecule has shown. Lately, the electronic properties of this molecule raised attention in the field of spintronics, specifically, the ability to act as a spin-filter. Nevertheless, the mechanism that controls this behavior is yet to be clarified; and in fact other properties such as conduction were experimentally tested, and while in some experiments it was observed that DNA acted as insulator, others observed semiconductor, conductor or superconductor behaviors. As an effort to continue this line of investigation and discover how to make new devices using DNA, this work tries to describe its electron transfer based on π orbitals on the B-form of this molecule by considering phonon and spin effects, which are present in physiological conditions where applications are most important. Using the two center approximation, the Envelope function, smoothing function, and the Tight Binding (TB) approach; two models were developed to study electron transfer (ET) in DNA. It was found that phonons have both relevance in intra and inter-helix ET, while spin-phonon interaction is found only intra-helix with spin-flip coupling. Optical phonons are coupled to electrons at first order while acoustic ones only couple to second order, thus optical modes are much more relevant. Intra-helix coupling with no spin-flip yields only a second order kinetic term thus the phonon and spin interactions don't affect this coupling. In conclusion, the model was able to make predictions qualitatively describing the persistence of coherence implied in experiments.

Keywords: Tight binding, deoxyribonucleic acid, electron transfer, electron-phonon, spin-phonon.

Contents

1 Introduction **2**
- 1.1 Structure of DNA . . . 2
- 1.2 DNA in the context of molecular spintronics . . . 4
- 1.3 Electron-phonon and spin-phonon interactions in DNA . . . 6
- 1.4 Hypothesis . . . 7
- 1.5 General and specific objectives . . . 7
  - 1.5.1 General objective . . . 7
  - 1.5.2 Specific objectives . . . 8

2 Methodology **9**
- 2.1 The tight binding model . . . 9
  - 2.1.1 TB with intrinsic spin-orbit coupling . . . 10
- 2.2 Two center approximation . . . 11
- 2.3 TB Hamiltonian with intrinsic spin-orbit coupling for DNA . . . 12
- 2.4 The envelope function approximation . . . 17

3 Results and Discussion **18**
- 3.1 DNA structure model . . . 18
- 3.2 Electron-phonon interaction in DNA . . . 19
- 3.3 Spin-phonon interaction in DNA . . . 27

4 Conclusions and future work **34**

Bibliography **35**

List of Figures **42**

Chapter 1

Introduction

Deoxyribonucleic acid (DNA) is a well known and investigated molecule due to its presence in almost all living cells, and its characteristic structure has encouraged its research in a variety of fields including biology, chemistry, medicine and physics. In biology, DNA sequencing is specially important for evolutionary relations and comparisons between species[1]. In chemistry, this molecule is studied for its interaction with others such as Deoxyuridine Triphosphate (dUTP), relevant in Polymerase chain reaction (PCR)[2]. In medicine, gene identification is a powerful tool to identify risk of illness related to hereditary factors[3]. In physics, scientists proposed the use of DNA in applications in electronic circuits when its self assembly and self recognition properties were discovered[4]. This was further promoted when experiments in this molecule showed high transfer rates of charge[5]. Researchers modeled the charge transfer using different methods such as tight binding[6] or *ab initio* calculations [7] to explain this behavior.

More recently, DNA has been deployed at the nanoscale for uses in self-assembly[8, 9], synthesis of polymers and nanomaterials[10] and others[11], giving birth to the field of DNA nanotechnology. The potential uses of this molecule include nanophotonics, theranostics, biophysics, synthetic biology, and more[12].

This chapter shows the context in which this work is based. First, the structure of DNA and its characteristics are presented. Next, the most relevant discoveries in molecular spintronics involving this molecule are discussed. Third, different studies of electron-phonon and spin-phonon interaction related to DNA are reviewed. Finally, the hypothesis and objectives of this thesis are written.

1.1 Structure of DNA

There are several forms of DNA depending on the base sequence and the environment, but B-form is the most common[13] and the one considered in this text. The structure is a double right handed helix polymer, where each helix is a polynucleotide chain oriented antiparallel with respect to the other, which gives it its chiral properties[14]. Nucleotides in this molecule are composed of a base, a sugar, and a phosphate group. The sugar and the phosphate group are common for all nucleotides but the change between different possible bases gives this molecule the ability to store information similarly to the on-off binary base in electronics.

There are four bases that can make up the nucleotides: Adenine (A), Thymine (T), Cytosine (C) and Guanine (G). The specific pattern of these bases in the chain form different DNA molecules. The double helix is connected through these bases via hydrogen

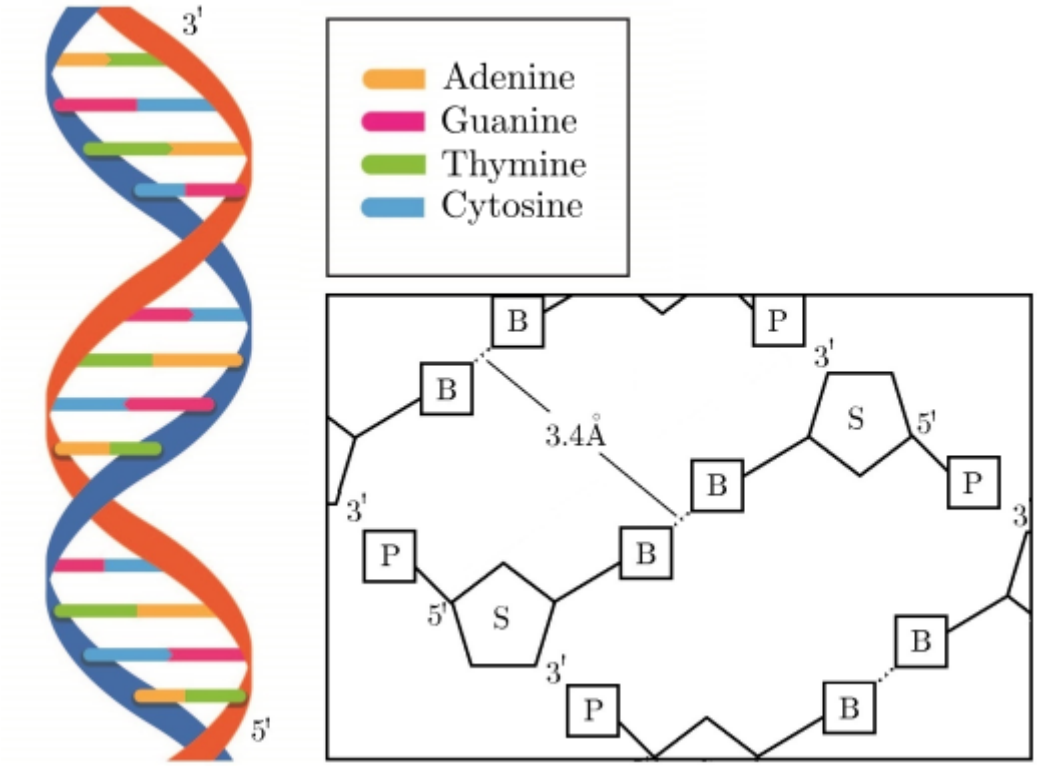

Figure 1.1: On the left, structure of the B-form DNA: a right handed double helix with ten nucleotides per turn (represented by colors as described in the top square). The chains are aligned in antiparallel orientations, where one chain goes from the $3'$ to the $5'$ sugar carbon and the other chain is reversed. In the right bottom square, a close-up of the structure can be seen. Bases are separated by a 3.4 Å translation along the helix axis. The phosphate group, the sugar and the base are represented as P, S and B respectively. The $3'$ and $5'$ sugar carbons are also represented[13].

bonding, which are only possible in the following pairs: A-T or C-G. In this bonding, Purines (A, G) provide the hydrogen bond donor and Pyrimidines (T, C) provide the acceptor[15].

The sugar associated to the DNA structure is a deoxyribose sugar, a five carbon compound between the base and the phosphate group. This component provides flexibility to the molecule due to its ability to twist and change between different shapes called sugar puckers[16]. Flexibility is important in this molecule to allow processes such as replication and packaging.

The phosphate group is exterior to the helix, providing structural support. Nucleotides are bonded through these phosphates groups in a bond from the $3'$ to the $5'$ sugar carbon of the next one, the $3'$-$5'$ phosphodiester bond[17]. The uniform exterior disposition allows proteins to recognize and bind to this molecule independently of its sequence, and the particular order of the bases provides a way to identify specific ones. Identification of these DNA-binding proteins is a topic of investigation by itself[18].

The B-form of DNA is presented in figure 1.1, and it is characterized by its asymmetric shape and antiparallel helices. The chains are both built from the $3'$ to the $5'$ sugar carbon but they are reversed with respect to each other. It has ten nucleotides per turn where each base pair is separated by 3.4 Å . This is also the form used in the research focused on the development of spin devices, spintronics[19].

1.2 DNA in the context of molecular spintronics

The study of spin and electron transfer is of great interest due to the potential advantages in emerging devices such as magnetoresistive random-access memory or spin-tunnel transistors[20]. This interest created the field of spintronics where the main concern is to investigate the ability to inject, manipulate and detect spin polarization and spin-polarized currents to storage and process information[21]. Initially, research focused on inorganic metals and semiconductors, and discoveries such as the ability to switch spin by spin-polarized currents, electric fields and photonic fields or spin dependent tunneling, increased the number of applications and the interest in this area[22].

As more materials were investigated, some experiments showed that organic materials can perform better in devices than inorganic metals and semiconductors, which encouraged their analysis and started the field of organic spintronics[23, 24, 25]. In a similar way, research on spin-transport discovered the advantages of studying individual molecules such as long relaxation times at low temperatures and long coherence times[26]. The aim of molecular spintronics is to study electron transport and to develop spintronics devices using single or few molecules.

Molecular spintronics started by investigating potential applications of molecules or by modifying existing spintronics devices using novel organic materials. One of these was DNA which stood out due to different useful and unique characteristics found including: ability to create synthetic chiral systems using DNA, spin polarization, spin dependent transport, long distance electron transfer, self assembly[27].

One example of modifying an existing device is the DNA spin-valve. Spin-valves are important devices developed by spintronics to read and record electronic information using the principle of spin-dependent transport[28], a type of electronic transport that changes depending on the spin of the electrons. This type of transport has been predicted using a tight-binding model of these molecules between ferromagnetic contacts, and a proposal of a DNA spin-valve was made[29]. The knowledge about the mechanism of charge transfer is increasing fast and it is revealing possible applications of the molecule of life as it is confirmed to be a plausible and effective component in molecular electronics.

Another area of interest in molecular spintronics is spin polarization. Before the field was developed, the most efficient way to manipulate the spin of a molecule was using a magnetic field that is applied externally or by passing a current through a ferromagnetic material[30]. Molecular spintronics continued to investigate other forms to achieve spin manipulation and found the capability of chiral molecules such as DNA to produce chiral-induced spin selectivity (CISS)[31]. The experimental observation of this phenomenon occurred in a setup consisting in a layer of DNA deposited on a gold surface. In figure 1.2 this experiment is illustrated; here, a linear polarized laser radiation was emitted through the DNA on the gold surface and no special interaction was observed (figure 1.2, left panel). Then the radiation, via the photoelectric effect, ejects unpolarized electrons from the gold surface that interact with DNA on the way out. In this step, the spin selectivity of DNA was observed as only electrons polarized with their spin aligned antiparallel to their velocity went trough, and reflected electrons went back to their initial state via tunneling (figure 1.2, right panel). Additionally, increasing the length of the DNA layer increased the polarization of the transmitted electrons[32]. This experiment is considered to be the starting point of DNA spintronics, but the mechanism of this interaction was yet to be clarified by further research[19].

In other experiments, conduction through double-stranded DNA oligomers was ob-

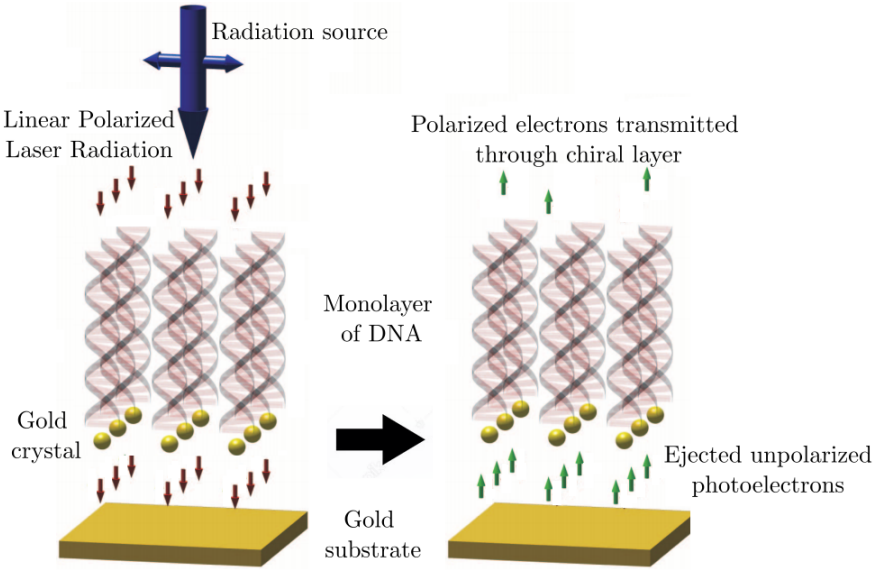

Figure 1.2: Experimental setup for the observation of spin polarization through DNA. The double stranded DNA was self-assembled on the gold crystal surface (golden balls). A linear polarized light (red arrows) passes unaffected by DNA and ejects unpolarized electrons (green arrows) from the gold substrate (left panel). Most electrons are spin filtered when passing trough the monolayer of DNA. Transmitted electrons are polarized with their spin aligned antiparallel to their velocity. Reflected electrons tunnel back to the substrate (right panel). Adapted from[32].

served to be spin selective at room temperature[33]. This effect was attributed to atomic spin–orbit coupling and to its chirality symmetry[34]. Accordingly in a recent work, chiral electric fields, arising from the chiral symmetry, were observed to induce chirality on spin currents via spin-orbit interaction[35]. After the observation of the spin selectivity of this molecule, a spin filter effect was theoretically predicted using an extended Peyrard–Bishop–Holstein model[36], a model used for the description of polaronic effects for charge migration in DNA nanowires[37]. In the model, the effect of external fields, temperature and sequence variation was analyzed and some peaks in polarization and pure spin currents were observed when these parameters were changed.

These results motivated the investigation of new devices and techniques for the synthesis of materials that can use the properties of DNA. For example, it was found that carbon nanotubes, helically wrapped with DNA, can create and detect spin-polarized carriers via spin–orbit coupling originated from the helical potential, and that their length increases such polarization[38]; and this discovery encouraged the development of techniques to synthesize longer nanotubes[39].

It has been shown that experiments and theoretical models demonstrated the potential application of DNA in new spintronics devices. Nevertheless the intrinsic mechanisms behind this are not completely understood[19]. To control the interaction of DNA with spin and use it in new devices, it is necessary to fully understand the mechanisms that produce the different experimental results and models. In the next section, different approaches to electron transport in DNA will be discussed.

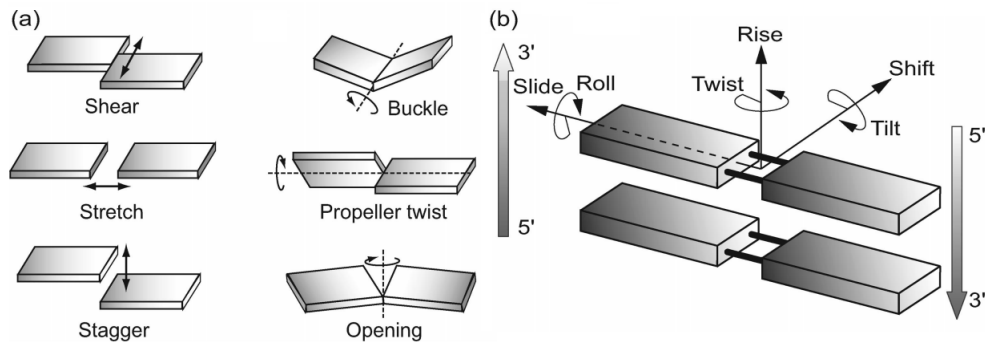

Figure 1.3: Translational and rotational symmetries of DNA bases in π stack geometry. a) DNA base pair degrees of freedom including shear, buckle, stretch, propeller twist, stagger and opening movements. b) DNA steps degrees of freedom including slide, roll, twist, rise, shift and tilt movements. Adapted from [55].

1.3 Electron-phonon and spin-phonon interactions in DNA

Electron transfer in this molecule is not a new subject under research and previous investigations take different points of view including chemistry, electrochemistry, physics, biology and more[40, 41, 42, 43]. Different applications have been suggested such as DNA chips, diagnosis, screening, and self assembly, among others; also, this molecule is believed to be a good structural component with versatility as a nanomaterial due to its biological functions, structure, biocompatibility, molecular recognition, and spin and electron transfer processes[44, 45].

Nevertheless, electron transfer in DNA had been a subject of debate in the past decades due to measurements of its electrical conductivity showing results from superconductivity to insulating behavior[5]. Another issue is the long distance electron transfer observed through DNA and explained as a process that occurs in multistep hopping, however, the mechanism is yet to be clarified[46, 47, 48, 49]. Common theoretical models at the time used tight-binding to explain this behavior, taking into account the charge carrier and molecular dynamics[50]. Also, other models were used such as *ab initio* calculations, DFT or Langevin equation[51, 52, 53].

Factors relevant in the electron transfer process are the vibrations, base sequence, the medium, temperature, spin and many other possible interactions with the electron or the structure. The base sequence is usually taken into account in experimental setups as well as the medium to obtain a desired result, but vibrations take a special place in the theoretical description of the electron transfer in DNA, since they are always present in biological applications and the rotational and translational movement of bases (see Figure 1.3) has been considered in conductivity studies of this molecule[54, 55]. Vibration occurs in different ways and modes, which can be represented as polarons, quasiparticles resulting of the interaction between electrons and the lattice, or some vibration modes such as DNA twisting and stretching modes can be represented as phonons[56], quasiparticles of vibrational energy required to move atoms in a lattice.

A recent study made a model of electron transfer in DNA with field theory in a system of π-electrons and phonons, and suggested some applications of luminescence quenching, electric current, and optical absorption[57]. Also, coherent delocalized phonon modes

involving the hydrogen bond between chains of DNA had been observed in physiological conditions[58], which are important in cyclization[59], a technique used to obtain information of the DNA bending[60].

Coherence of the electron transfer process is also a concern in DNA since it allows the long distance charge transfer previously remarked. A study found that coherent motion of large polarons is the dominant mechanism of charge transfer in this molecule[61], result that could explain the long distance charge transfer. This was supported by a recent approach with no particular base sequence that concluded that optical phonons are predominant over acoustical ones and large polarons are expected in DNA[62]. Briefly, polarons are closely related to phonons as both represent a change in the atom position and they have been also studied to explain electron transfer in this molecule[63].

Now that the spin and phonon interaction with electron transfer in DNA has been reviewed, the interaction between them needs to be addressed. Spin-phonon coupling affects electron transport properties since this has been used in spin mechanical setups for quantum science and technology, and being able to manipulate this coupling is of special interest[64].

This interaction is important since phonons can drive spin lattice relaxation, a process that limits the coherence time, a primary concern in the quantum computing field[65] and some experiments have focused in achieving long relaxation times to allow coherent spin manipulation and quantum entanglement[66, 67]. Raman scattering is usually used to measure spin-phonon interactions[68, 69] but investigation of more ways to analyze this interaction are at their infancy. For example, determining the angular momentum of phonons is a potential method to study the spin-phonon interaction[70, 71] which can be used to study it in DNA.

Spin-phonon interaction is being studied in crystals and other materials to analyze their magnetoelectric properties[69, 72, 73, 66], but in the case of DNA the literature about this subject is still limited[74, 75]. The electron transfer process mediated by the spin-phonon interaction remains to be discussed. Motivated by this, in this work a tight binding description of the electron-phonon and spin-phonon interactions in electron transfer in DNA is developed. With this goal, a basis of π orbitals per base for the tight binding description is used, and a wave function by using the envelope function approximation is proposed. The phonons are included through a variation of the hopping parameters as Ishikawa and Suzuura had done[76, 77]. Our results will be compared with experimental and theoretical results found in the literature.

1.4 Hypothesis

A tight binding (TB) model based on π orbitals and combined with the envelope function approximation, can be used to describe the electron-phonon and spin-phonon interactions in electron transfer in DNA.

1.5 General and specific objectives

1.5.1 General objective

To describe, by using a TB model, the electron-phonon and spin-phonon interactions in electron transfer in DNA

1.5.2 Specific objectives

- To use the envelope function approximation for writing the wave function of electrons in DNA including the interaction with phonons
- To include the spin in the previous model through the intrinsic spin-orbit interaction
- To compare the results obtained in the two previous steps, with experimental and theoretical results found in the literature
- To analyze the results in terms of the influence of the electron-phonon and the spin-phonon interaction in electron transfer in DNA

Chapter 2

Methodology

The tools needed to accomplish the objectives will be presented in this chapter. First, the nature of the tight binding model and how it is used to describe the electron transfer is explained. Then the two center approximation used to facilitate the calculations is presented. After this, an approximation to allow the model to have a wider description of the ET is described. Finally, the hopping parameters for DNA used in the models will be showed.

2.1 The tight binding model

Tight binding model (TB) is an interpolation method used to study the electron transfer of a periodic material by making a linear combination of atomic orbitals at the sites in the lattice[78]. This method can be applied to different materials with a periodic lattice and it is based on the translational symmetry of such structures. Solutions for the Schrödinger equation for a periodic potential have a special form given by Bloch's theorem expressed as: $\psi_{\boldsymbol{k}}(\boldsymbol{r}) = u_{\boldsymbol{k}}(\boldsymbol{r})e^{i\mathbf{k}\cdot\mathbf{r}}$, where $u_{\boldsymbol{k}}(\boldsymbol{r}) = u_{\boldsymbol{k}}(\boldsymbol{r}+\boldsymbol{T})$ has the periodicity of the lattice and $\boldsymbol{T}$ is a translation vector[79]. By assuming the influence of one lattice site to another to be small, the wavefunction for one electron in the j^{th} orbital satisfying the Bloch theorem is:

$$\psi_j(\boldsymbol{k},\mathbf{r}) = \frac{1}{\sqrt{N}}\sum_{\mathbf{R}}^{N} e^{i\mathbf{k}\cdot\mathbf{R}}\psi_j(\mathbf{r}-\mathbf{R}),$$

where $\mathbf{R}$ is the position of the atom in the lattice and N is the number of unit cells (or sites for a monoatomic basis)[79]. In general, the electronic wavefunction is a linear superposition of Bloch functions in all N sites:

$$\psi_j(\mathbf{k},\mathbf{r}) = \sum_{l=1}^{n} c_{j,l}(\mathbf{k})\phi_{\mathbf{l}}(\mathbf{k},\mathbf{r}), \tag{2.1}$$

where $c_{j,l}$ are the coefficients of the expansion and ϕ_l is the lth Bloch function.

The energy $E_j(\mathbf{k})$ of the jth band is given by:

$$E_j(\mathbf{k}) = \frac{\langle\Psi_j|\mathcal{H}|\Psi_j\rangle}{\langle\Psi_j|\Psi_j\rangle}, \tag{2.2}$$

where $\mathcal{H}$ is the Hamiltonian operator of the system under study [80], that without spin-orbit interaction is:

$$\mathcal{H} = -\frac{\hbar^2\nabla^2}{2m} + V_{at}(\mathbf{r}), \tag{2.3}$$

where the first term is the kinetic energy of the electrons and the second one is the atomic potential. Substituting Eq. 2.1 into Eq. 2.2 gives:

$$E_j(\mathbf{k}) = \frac{\sum_{i,l}^{n} c_{ji}^* c_{jl} \langle \Phi_i | \mathcal{H} | \Phi_l \rangle}{\sum_{i,l}^{n} c_{ji}^* c_{jl} \langle \Phi_i | \Phi_l \rangle} = \frac{\sum_{i,l}^{n} H_{il} c_{ji}^* c_{jl}}{\sum_{i,l}^{n} S_{il} c_{ji}^* c_{jl}}, \tag{2.4}$$

where H_{il} is called the transfer integral and S_{il} is called the overlap integral, and they are defined by:

$$H_{il} = \langle \Phi_i | \mathcal{H} | \Phi_l \rangle, \qquad S_{il} = \langle \Phi_i | \Phi_l \rangle. \tag{2.5}$$

When the values of the $n \times n$ transfer and overlap matrices are fixed for a given $\mathbf{k}$ value, the coefficient c_{ji}^* is optimized to minimize the energy, $E_j(\mathbf{k})$. By taking a partial derivative of $E_j(\mathbf{k})$ with respect to c_{jm}^*, the local minimum condition is set to zero so:

$$\frac{\partial E_j(\mathbf{k})}{\partial c_{jm}^*} = \frac{\sum_{l}^{n} H_{ml} c_{jl}}{\sum_{i,l}^{n} S_{il} c_{ji}^* c_{jl}} - \frac{\sum_{i,l}^{n} H_{il} c_{ji}^* c_{jl} \sum_{l}^{n} S_{ml} c_{jl}}{(\sum_{i,l}^{n} S_{il} c_{ji}^* c_{jl})^2} = 0,$$

where $\sum_{i,l}^{n} S_{il} c_{ji}^* c_{jl}$ is a common factor and the second term contains $E_j(\mathbf{k})$ as Eq. 2.4. After simplifying, it is obtained:

$$\sum_{l=1}^{n} H_{ml} c_{jl} = E_j \sum_{l=1}^{n} S_{ml} c_{jl}.$$

In a general way, it can be written:

$$H = \begin{pmatrix} H_{11} & H_{12} & \cdots & H_{1n} \\ H_{21} & H_{22} & \cdots & H_{2n} \\ \vdots & \vdots & \ddots & \vdots \\ H_{n1} & H_{n2} & \cdots & H_{nn} \end{pmatrix}, S = \begin{pmatrix} S_{11} & S_{12} & \cdots & S_{1n} \\ S_{21} & S_{22} & \cdots & S_{2n} \\ \vdots & \vdots & \ddots & \vdots \\ S_{n1} & S_{n2} & \cdots & S_{nn} \end{pmatrix}, \psi_j = \begin{pmatrix} c_{j1} \\ c_{j2} \\ \vdots \\ c_{jn} \end{pmatrix},$$

and:

$$H\psi_j = E_j S \psi_j,$$

thus the energies E_j can be calculated by solving the secular equation[81]:

$$\det(H - E_j S) = 0. \tag{2.6}$$

2.1.1 TB with intrinsic spin-orbit coupling

The effect of the spin arises from the interaction of the magnetic moment of the electron with the effective magnetic field due to its motion around the nucleus. The spin–orbit interaction is introduced into the Hamiltonian with the spherical potential approximation as the following extra term:

$$\mathcal{H}_{SO} = \xi(r) \mathbf{L} \cdot \mathbf{S}, \tag{2.7}$$

where $\xi(r)$ is the coupling constant, $\mathbf{L}$ is the orbital angular momentum and $\mathbf{S}$ is the spin angular momentum[82, 83], and with:

$$\xi(r) = \frac{1}{2m_e^2 c^2} \frac{1}{r} \frac{dV}{dr}.$$

This extra term affects the value of the transfer integrals calculated with the two center approximation and the terms arising from this need to be addressed. To do this, the extra

	$\|p_x\rangle$	$\|p_y\rangle$	$\|p_z\rangle$
$\langle p_x\|$	0	$-is_z\xi_p$	$is_y\xi_p$
$\langle p_y\|$	$is_z\xi_p$	0	$-is_x\xi_p$
$\langle p_z\|$	$-is_y\xi_p$	$is_x\xi_p$	0

Table 2.1: Expectation values for intrinsic SO coupling considering p orbitals. Here, s_x, s_y, s_z is the contribution of the Pauli spin matrices in directions x, y, z, and ξ_p is the coupling constant for p orbitals[81].

term of the Hamiltonian, Eq. 2.7, is substituted in the definition of the transfer integral, Eq. 2.5. Here, the orbitals $\phi_{i,l}$ are expressed in the $|l, m_l\rangle$ basis as:

$$|p_x\rangle = -\frac{1}{\sqrt{2}}(|1,1\rangle - |1,-1\rangle), \quad |p_y\rangle = \frac{i}{\sqrt{2}}(|1,1\rangle + |1,-1\rangle), \quad |p_z\rangle = |1,0\rangle,$$

so the transfer integral results in:

$$H_{il} = \langle l, m|\xi(r)\mathbf{L}\cdot\mathbf{S}|l', m'\rangle.$$

Then the possible combination of orbitals with the SO Hamiltonian can be obtained. These values are presented in table 2.1.1 where $\xi_p = \xi(r)\hbar/2$. These terms will appear in the calculation of the intrinsic SO coupling contribution together with the SK parameters, obtained by using the two center approximation.

2.2 Two center approximation

Calculations of the matrix elements to find the transfer integral in Eq. 2.5 can be extremely difficult, because the atomic potential in the Hamiltonian operator of Eq. 2.3 contains contributions from multiple atoms in the lattice. One simplification is to consider only contributions from the two atoms involved in the electronic transition, this is called the two center approximation[78]. Then the Hamiltonian operator with this approximation is:

$$\mathcal{H} = -\frac{\hbar^2\nabla^2}{2m} + \sum_{ij} V_{at}(\mathbf{R}_i - \mathbf{R}_j),$$

with $\mathbf{R}_i$ and $\mathbf{R}_j$ being the position of the i and its first neighbor j.

By considering the vector connecting both atoms as an axis similar to that of a diatomic molecule, each of the functions ϕ can be expressed as a sum of functions space quantized with respect to that axis. Then, if ϕ were an atomic p orbital, it can be expressed as a linear combination of a p_σ and a p_π function with respect to the axis[78]. For example, in terms of the energy for the case of p_z orbitals, the hopping integral has an energy V divided in two: $V_{pp\sigma}$ and $V_{pp\pi}$, the first a pure σ bond between p orbitals, and the second a pure π bond between p orbitals. Here, the first and second sub indexes refer to the first and second orbital and the last sub index indicates the type of bonding.

The energy integrals in terms of the two center integral can be obtained in tables or calculated by defining the cosine directors $l = \sin\beta\cos\alpha$, $m = \sin\beta\sin\alpha$, $n = \cos\beta$ in the plane where the two atoms are; here, β is the angle between the vector connecting the atoms and the vertical axis, and α is the angle between the projection of the vector

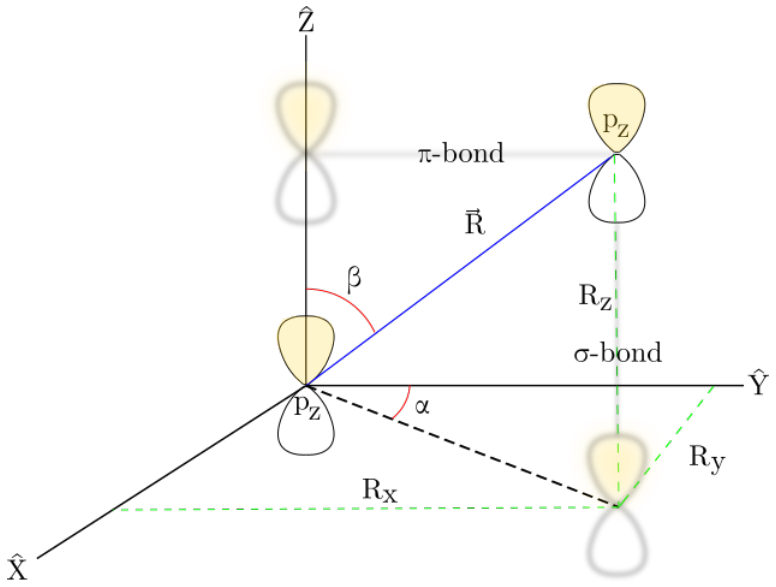

Figure 2.1: Example of the two center approximation for p_z orbitals. The bonding between these orbitals is considered to be a combination of a π-bond and a σ-bond, where the "amount" of each bonding is determined by the connecting vector $\hat{R}$. The angle between this vector and the vertical axis is β, and the angle between the Y axis and the projection of $\hat{R}$ onto the horizontal plane is α.

connecting the sites onto the horizontal plane and the Y axis; an example can be seen in figure 2.1. Then each component of V is the result of the linear combination of all types of bonding where the coefficients are written in terms of l, m and n.

2.3 TB Hamiltonian with intrinsic spin-orbit coupling for DNA

To obtain the TB Hamiltonian for DNA, it is necessary to understand the structure considered for this molecule, the orbitals participating in the electronic transitions, and their couplings. This was already done by Varela et al.[81], thus the structure used in this work needs to be presented.

The structure used to determine the Hamiltonian can be seen in figure 2.2. Here, only one helix is represented but a double helix is considered. The radius is represented by a, the pitch is b and the angle between bases is $\Delta\phi$. The orbitals considered are s, p_x, p_y and p_z and they are oriented following the rotating basis axis; the sites are uniformly distributed in the helix to sum a total of N per helix and $2N$ in total. Finally, each base has one unpaired mobile electron in the $2p_z$ orbital. Then having in mind this structure, the procedure to obtain the Hamiltonian follows.

To obtain the TB Hamiltonian, one should have a wavefunction defined. Varela et al. cosidered this wavefunction:

$$|\Psi\rangle = \sum_{\rho,i} a_{\rho,i} c^{\dagger}_{\rho,i} |0\rangle,$$

where i is the site,$c^{\dagger}$ is the fermion creation operator, and the orbitals are represented as

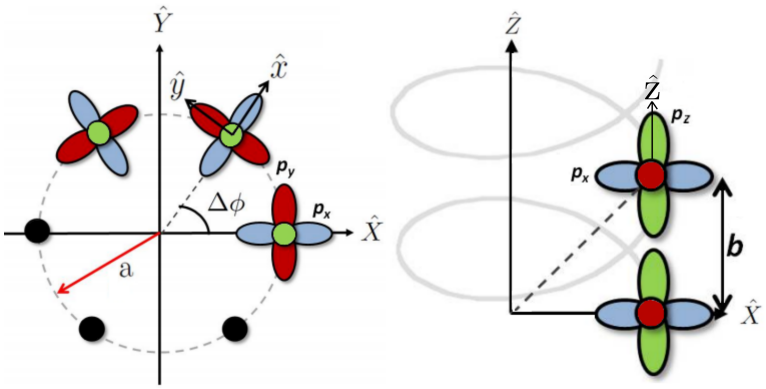

Figure 2.2: Structure of the double helix DNA from Varela et al. considered in the determination of the TB Hamiltonian with intrinsic spin-orbit coupling. Here, the orbital orientation is shown and each orbital is distinguished by colors: p_x is blue, p_y is red and p_z is green. Black dots represent other sites with orbitals. Parameters a and b are the radius and pitch of the helix respectively, and $\Delta\phi$ is the angle between bases. There are two set of axis: one is the fix basis $\{X,Y,Z\}$ and the other is the rotating basis $\{X,y,z\}$. Adapted from[81].

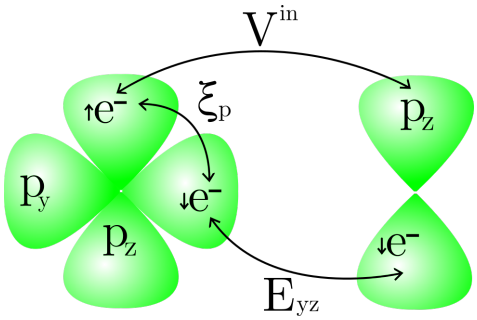

Figure 2.3: Electron movement with the intrinsic SO effect. The electron at a p_z orbital moves to either a p_x or p_y orbital in the same site while changing its spin, then moves to another site into the p_z orbital with no spin change. Overall, the electron moves from one p_z orbital to another with the intra-helix coupling parameter V^{in}. The movement to the p_x orbital is not drawn to improve recognition of the electron transitions.

ρ. Then the coupling of the wavefunction with an orbital, ρ, is given by:

$$\langle\rho(i)|\mathcal{H}|\Psi\rangle = \epsilon a_{\mu,i},$$

where ϵ is the Hamiltonian eigenvalue with all interactions and $a_{\mu,i}$ is the amplitude of orbital μ in site i. Therefore, to obtain the TB Hamiltonian, one should consider all the couplings present.

The coupling terms in the intrinsic SO contribution includes both Slater and Koster (SK) and intrinsic SO parameters thus both need to be taken in account to calculate the hopping integrals $V_o^{in,out}$. This coupling is represented in figure 2.3, where electrons at a p_z orbital are transferred to a $p_{x,y}$ orbital of the same site while flipping the spin. Then they move to another p_z orbital of the nearest site[81]. First, the SK parameters will be addressed.

By using the two center approximation, the values for the transfer integrals are substituted by parameters: V_{ll}^m, whose values are constants obtained from the literature. These

are defined as the SK parameters by the following equation:

$$V_{ll}^{m}\delta_{mm'} = \langle l', m', \mathbf{R}|\hat{\mathcal{H}}|l, m, \mathbf{R}\rangle,$$

where $\mathbf{R}$ is the position of the orbital, and l and m are the angular momentum and magnetic quantum numbers respectively; here, the first number describes orbitals ϕ_i and ϕ_j and the second describes the type of bonding: σ, π. Nevertheless this parametrization is only applicable when both orbitals are aligned to form the specific type of bonding, σ or π in this case. Then in a coupling where orbitals are not aligned, the SK parameters are calculated as described in the previous section where the overlap energy $E^{i,j}_{\phi_i,\phi_j}$ between i and j sites is a combination of bondings. Also, it is important to know that the parameters satisfy: $\langle l|\mathcal{H}|l'\rangle = (-1)^{l+l'}\langle l'|\mathcal{H}|l\rangle$[81], to easily obtain the reverse coupling.

By considering only the p orbitals, there are only two parameters for the approximation: V^{π}_{pp} and V^{σ}_{pp}. The aligning for the π and σ bondings can be seen in figure 2.1, and it is clear that in an arbitrary alignment of orbitals both bondings are present, and this is the case for the DNA intra helix couplings. The determination of the values of these parameters is usually made by matching them to the results obtained by other methods[84], but Harrison, in an empirical finding, found that these parameters can be obtained from the following equation:

$$V_{\phi_i,\phi_l} = \kappa_{\phi_i,\phi_l}\frac{\hbar^2}{m_e d^2},$$

where d is the inter-nuclear distance, the value of $\hbar^2/m_e$ is 7.62 eVÅ, and κ is a dimensionless coupling constant with $\kappa_{pp\pi} = 0.81$ and $\kappa_p p\sigma = 3.24$[85]. Also, this approximation is only valid for near equilibrium positions, thus phonons in this work are considered to cause only little vibrations.

To obtain the linear combination of SK parameters, Ando proposed the scenario in figure 2.4a) where the overlap energy is given by:

$$E^{i,j}_{\phi_i,\phi_j} = (\mathbf{n}(\phi_i)^{\parallel}, \mathbf{n}(\phi_j)^{\parallel})V^{\sigma}_{pp} + (\mathbf{n}(\phi_i)^{\perp}, \mathbf{n}(\phi_j)^{\perp})V^{\pi}_{pp}, \tag{2.8}$$

where $\mathbf{n}(\phi_i)^{\parallel}$ is the projection of $\mathbf{n}(\phi_i)$ onto the vector connecting the sites, $\mathbf{R}_{ji} = \mathbf{R}_j - \mathbf{R}_i$, and $\mathbf{n}(\phi_i)^{\perp}$ is the projection onto a plane perpendicular to $\mathbf{R}_{ji}$[86]. These coefficients represent how aligned are the orbitals to form the particular σ or π bonding. The unit direction $\mathbf{n}(\phi_i)^{\parallel}$ is calculated with the dot product between $\mathbf{n}(\phi_i)$ and $\mathbf{R}_{ji}$ and normalizing in the direction of $\mathbf{R}_{ji}$ as:

$$\mathbf{n}(\phi_i)^{\parallel} = \frac{(\mathbf{R}_{ji}, \mathbf{n}(\phi_i)}{(\mathbf{R}_{ji}, \mathbf{R}_{ji})}\mathbf{R}_{ji},$$

and the perpendicular direction is the remaining of the unit direction after the subtraction of the parallel direction:

$$\mathbf{n}(\phi_i)^{\perp} = \mathbf{n}(\phi_i) - \frac{(\mathbf{R}_{ji}, \mathbf{n}(\phi_i)}{(\mathbf{R}_{ji}, \mathbf{R}_{ji})}\mathbf{R}_{ji};$$

then Eq. 2.8 can be written as:

$$E^{i,j}_{\phi_i,\phi_j} = (\mathbf{n}(\phi_i), \mathbf{n}(\phi_j))V^{\pi}_{pp} + \frac{(\mathbf{R}_{ji}, \mathbf{n}(\phi_i)(\mathbf{R}_{ji}, \mathbf{n}(\phi_j)}{(\mathbf{R}_{ji}, \mathbf{R}_{ji})}(V^{\sigma}_{pp} - V^{\pi}_{pp}).$$

With this equation, one can obtain the expressions for the desired coupling. The unit directions of the orbitals in DNA in the fix system basis are: $\mathbf{n}(p_x) = \cos(\phi)\hat{X} + \sin(\phi)\hat{Y}$,

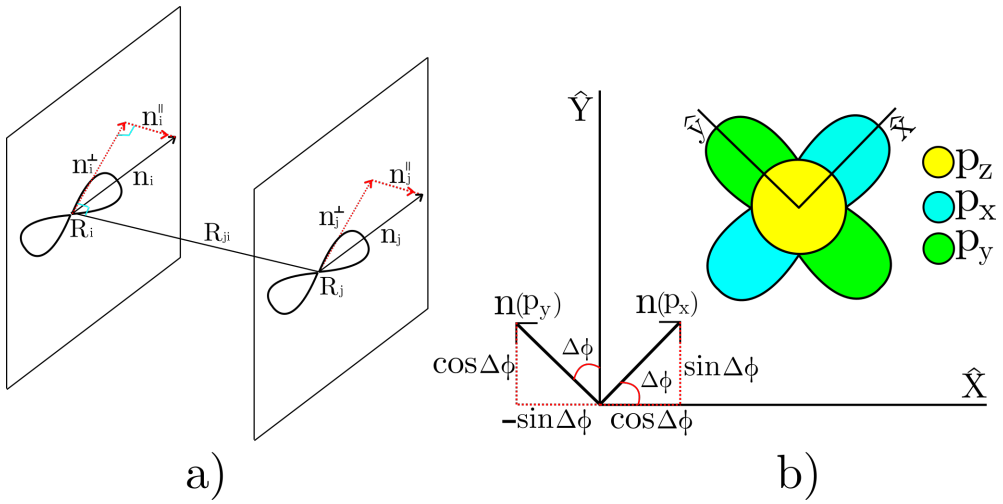

Figure 2.4: a) Here, the i and j orbitals are represented on $\mathbf{n}_i$ and $\mathbf{n}_j$ unit directions. These directions are independent on each other and their joining vector, $\mathbf{R}_{ji}$. The unit vectors, $\mathbf{n}_{i,j}$, are divided in parallel components with $\mathbf{R}_{ji}$, $\mathbf{n}(\phi_i)^{\parallel}$ and $\mathbf{n}(\phi_j)^{\parallel}$, and perpendiculars, $\mathbf{n}(\phi_i)^{\perp}$ an $\mathbf{n}(\phi_j)^{\perp}$. Then the σ bonding, which is produced when the orbitals follow the parallel direction, is the combination of $\mathbf{n}(\phi_i)^{\parallel}$ and $\mathbf{n}(\phi_j)^{\parallel}$ components; and the π bonding is the combination of the perpendicularly aligned orbitals. b) Description of the unit directions of p_x, p_y and p_z orbitals in the XY plane. These are divided in their fix basis components to be used in the calculation of SK parameters. The p_z is completely in $\hat{Z}$ while p_x and p_y have components in $\hat{X}$ and $\hat{Y}$ directions.

$\mathbf{n}(p_y) = -\sin(\phi)\hat{X} + \cos(\phi)\hat{Y}$, and $\mathbf{n}(p_z) = \hat{Z}$, with $\phi = (i-1)\Delta\phi$. The terms for p_x and p_y are represented in figure 2.4b), and the term $\mathbf{n}(p_z)$ is trivial to obtain since its direction is only on $\hat{Z}$.

In relation, this can be used to calculate the term for the kinetic intra-helix. Here, the p_z orbital of the i site will couple only with the p_z orbital of the j site, then the energy associated is:

$$E_{zz}^{ij} = V_{pp}^{\pi(in)} + \frac{b^2\Delta\phi^2(V_{pp}^{\sigma(in)} - V_{pp}^{\pi(in)})}{4\pi^2|\mathbf{R}_j i|^2} = t_o^{in}.$$

The inter-helix coupling is easily obtained as both orbitals are aligned for a complete π bond, thus $E_{zz}^{ij} = V_{pp}^{\pi(out)} = t_o^{out}$.

Continuing with the calculation of the TB Hamiltonian with intrinsic SO coupling, it has been observed that it has both SK and intrinsic SO terms. SK parameters arise from the inter-site coupling and intrinsic SO terms come from intra-site couplings. Let's consider first the inter-site coupling. The SK parameters that will be needed are E_{xz}^{ij} and E_{yz}^{ij} since the electrons move only between p_z and $p_{x,y}$ orbitals of different sites. Their calculated expressions are:

$$E_{xz}^{ij} = \frac{2ab\sin^2(\frac{\Delta\phi}{2})(\phi_i - \phi_j)(V_{pp}^{\sigma} - V_{pp}^{\pi})}{2\pi|\mathbf{R}_{ji}|^2} = -E_{zx}^{ij},$$
$$E_{yz}^{ij} = \frac{ab\sin(\phi_j - \phi_i)(\phi_j - \phi_i)(V_{pp}^{\sigma} - V_{pp}^{\pi})}{2\pi|\mathbf{R}_{ji}|^2} = E_{zy}^{ij}.$$

The energy for the intra-site spin-flip process caused by the intrinsic SO, can be

described using table 2.1.1; where, for the structure of DNA described:

$$s_x = \sigma_x \cos(\phi_l) + \sigma_y \sin(\phi_l), \quad s_y = -\sigma_x \sin(\phi_l) + \sigma_y \cos(\phi_l), \quad s_z = \sigma_z,$$

where $\sigma_{x,y,z}$ are the Pauli matrices[81]. This table contains the expectation values for this coupling needed to write the orbital coupling equations. These take in account all possible electron couplings previously described with both SO and SK parameters:

$$\begin{aligned}
(\epsilon - \epsilon_{2p}^{\sigma}) a_{xi} &= i s_y \xi_p a_{zi} + \sum_{j=1}^{2} E_{xz}^{ij} b_{zj}, \\
(\epsilon - \epsilon_{2p}^{\sigma}) a_{yi} &= -i s_x \xi_p a_{zi} + \sum_{j=1}^{2} E_{yz}^{ij} b_{zj}, \\
(\epsilon - \epsilon_{2p}^{\pi}) a_{zi} &= i s_x \xi_p a_{yi} - i s_y \xi_p a_{xi} + \sum_{j=1}^{2} \sum_{x,y} E_{z(x,y)}^{ij} b_{(x,y)j}, \\
(\epsilon - \epsilon_{2p}^{\sigma}) b_{xj} &= i s_y \xi_p b_{zj} + \sum_{jj'=1}^{2} E_{xz}^{jj'} a_{zjj'}, \\
(\epsilon - \epsilon_{2p}^{\sigma}) b_{yj} &= -i s_x \xi_p a_{zj} + \sum_{jj'=1}^{2} E_{yz}^{jj'} a_{zjj'},
\end{aligned} \tag{2.9}$$

where $\epsilon_{2p}^{\sigma,\pi}$ is the site energy for $p_{x,y}$ (σ) and p_z (π) orbitals, $a_{(x,y,z)i}$ is the amplitude of the orbital at site i, and b refers to neighboring sites. To explain how these equations were written, consider the first equation: in the left hand side the orbital amplitude for the p_x in the i site, a_{xi}, is multiplied by the energy available to transfer the electron; and in the right hand side, the energies required for the electron to transfer to the other orbitals in all possible couplings are written. The solution to these equations leads to: $V_o^{in} = \lambda_{SO}^{in} \nu_l$, where:

$$\lambda_{SO}^{in} = \frac{4\pi \xi_p ab \Delta\phi (1 - \cos(\Delta\phi))(V_{pp}^{\sigma(in)} - V_{pp}^{\pi(in)})}{(\epsilon_{2p}^{\pi} - \epsilon_{2p}^{\sigma})(8\pi^2 a^2 (1 - \cos(\Delta\phi) + b^2 \Delta\phi^2))};$$

so the TB Hamiltonian for the intrinsic SO interaction in the intra-helix is[81]:

$$\mathcal{H}_{SO}^{in} = i\lambda_{SO}^{in} \sum_{ij} c_i^{\dagger} \nu_{ij} s_y c_j.$$

The inter-helix intrinsic SO coupling is zero at first order because the p_z and $p_{x,y}$ orbitals at different sites are completely miss-aligned for this coupling in the two center approximation, thus: $V_o^{out} = 0$ and $\mathcal{H}_{SO}^{out} = 0$.

The calculated terms are added to obtain the real space Hamiltonian. Then its derivation in the reciprocal space is done by following the procedure in the tight binding model section (2.1), so the full Hamiltonian for the half filled p_z orbital at the surroundings of the symmetry points, $\mathbf{K}_\nu = (\nu \frac{\pi}{2R}, 0)$, obtained by Varela et al. is:

$$\begin{aligned}
\mathcal{H} = &- 2\nu q_y R t^{in} \mathbf{1}_{\sigma'} \mathbf{1}_s + t^{out} {\sigma'}_x \mathbf{1}_s - 2\nu \lambda_{SO}^{in} \mathbf{1}_{\sigma'} s_y \\
&- 2\nu q_y R \lambda_R^{in(1)} \mathbf{1}_{\sigma'} s_y - 2\nu \lambda_R^{in(2)} \mathbf{1}_{\sigma'} s_x - \lambda_R^{out} {\sigma'}_y s_y,
\end{aligned} \tag{2.10}$$

where $\nu = \pm$, q_y is a wave vector around $\mathbf{K}_\nu$, λ_R is the Rashba coupling, and $\mathbf{1}_{\sigma',s}$ refers to the unit matrices in pseudo-spin and spin space. This result will used to compare the ones obtained in the next chapter.

Now that the hopping integrals that will be used in the model are defined and their origin is explained, the envelope function approximation is introduced to explain the wavefunctions that will be considered.

2.4 The envelope function approximation

The Schrödinger equation in a periodic lattice potential $V_L(\mathbf{r})$ under the influence of a slowly varying external potential $V(\mathbf{r})$ is:

$$\left[\frac{p^2}{2m_e} + V_L(\mathbf{r})\right]\Psi(\mathbf{r}) + V(\mathbf{r})\Psi(\mathbf{r}) = E\Psi(\mathbf{r}). \tag{2.11}$$

This has to be solved to calculate the bulk band structure of the material. The solutions of Eq. 2.11 are Bloch waves of the form: $\Psi_{n\mathbf{k}}(\mathbf{r}) = Nu_{n\mathbf{k}}(\mathbf{r})e^{i\mathbf{kr}}$, where n is the band index, N is the normalization factor and $u_{n\mathbf{k}}(\mathbf{r})$ are lattice-periodic functions. This function has two parts and can be written as:

$$\Psi(\mathbf{r}) \approx u_{\mathbf{k}}(\mathbf{r})F(\mathbf{r}), \tag{2.12}$$

where $u_{\mathbf{k}}(\mathbf{r})$ is the Bloch function, a fast oscillating part with the periodicity of the lattice; and $F(\mathbf{r})$ is the plane wave, a slowly varying part called the envelope function and is only applicable in high-symmetry points of the Brillouin zone[87, 88]. Using Eq. 2.12, the equation for the envelope function considering only the n-th band is:

$$E_n(-i\Delta)F(\mathbf{r}) + V(\mathbf{r})F(\mathbf{r}) = EF(\mathbf{r}),$$

where $E_n(-i\Delta)$ is the operator obtained by replacing $\mathbf{k}$ by $-i\Delta$ in the dispersion relation[62].

In a two site basis the wavefunction is written as the superposition of two sites as:

$$\Psi(\mathbf{r}) = \sum_{\mathbf{R}_A}\Psi_A(\mathbf{R}_A)\psi(\mathbf{r}-\mathbf{R}_A) + \sum_{\mathbf{R}_B}\Psi_B(\mathbf{R}_B)\psi(\mathbf{r}-\mathbf{R}_B), \tag{2.13}$$

where $\psi(\mathbf{r}-\mathbf{R}_{A,B})$ are the atomic orbitals centered at the A and B sites. Substituting Eq. 2.13 into Eq. 2.11, the expectation value of the Hamiltonian is:

$$\begin{aligned} -\gamma_o\sum_l \Psi_A(\mathbf{R}_A-\tau_l) &= (E-E_B)\Psi_B(\mathbf{R}_B), \\ -\gamma_o\sum_l \Psi_B(\mathbf{R}_B+\tau_l) &= (E-E_A)\Psi_A(\mathbf{R}_A), \end{aligned}$$

where γ_o is the nearest neighbor overlap integral, and τ_l are the vectors connecting the sites[62]. Then the wavefunctions used for the nearest neighbor tight-binding model in a two sites system are:

$$\Psi_A(\boldsymbol{R}_A) = e^{i\boldsymbol{K}\cdot\boldsymbol{R}_A}F_A^{\boldsymbol{K}}(\boldsymbol{R}_A) + e^{i\boldsymbol{K}'\cdot\boldsymbol{R}_A}F_A^{\boldsymbol{K}'}(\boldsymbol{R}_A), \tag{2.14}$$

and:

$$\Psi_B(\boldsymbol{R}_B) = e^{i\boldsymbol{K}\cdot\boldsymbol{R}_B}F_B^{\boldsymbol{K}}(\boldsymbol{R}_B) + e^{i\boldsymbol{K}'\cdot\boldsymbol{R}_A}F_B^{\boldsymbol{K}'}(\boldsymbol{R}_B). \tag{2.15}$$

Chapter 3

Results and Discussion

This chapter follows the development of the TB models for DNA taking into account the lattice phonons and the intrinsic spin-orbit interaction. First, the structure model used is described. Then, the TB model for electron-phonon interaction is built and developed. Finally, the TB model for the phonon and spin-orbit, or spin-phonon, interaction is presented and solved.

3.1 DNA structure model

As reviewed, DNA is present in nature in many forms thus it is important to consider which form will be used in the model. In relevance with phonon and spin-orbit interactions in physiological conditions and no specific base sequence (electron transport is expected to be nearly sequence independent[43]), B-form DNA was chosen as the basic structure for the model, which is the usual form this molecule takes. The structure was modeled

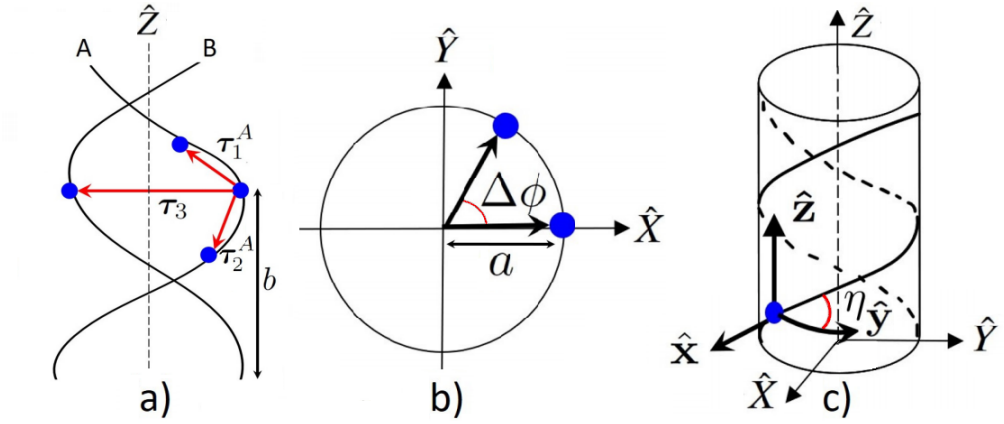

Figure 3.1: Structure of the double helix model of DNA in the fixed basis $\{X,Y,Z\}$. a) Side view with intra-helix, $\tau_{1,2}^{A,B}$, and inter-helix, τ_3, base vectors and pitch, b. b) Top view of a helix with rotation angle between two intra-helix bases, $\Delta\phi$, and radius, a. c) 3D view with chiral angle, η, and rotating system basis vectors $\{x,y,z\}$. Adapted from[62].

with 2N nucleotides simplified as 2N sites of s and p orbitals connected with base vectors, τ. The model is a right handed double helix in a fixed basis, $\{X,Y,Z\}$, defined in figure 3.1, where $\hat{Z}$ is in the helix direction and $\hat{X}$ and $\hat{Y}$ are perpendicular. A rotating system or local basis is also defined in figure 3.1c), where $\hat{x}$ is in the radial direction, $\hat{y}$ is in the arc direction, and $\hat{z}$ is parallel to $\hat{Z}$.

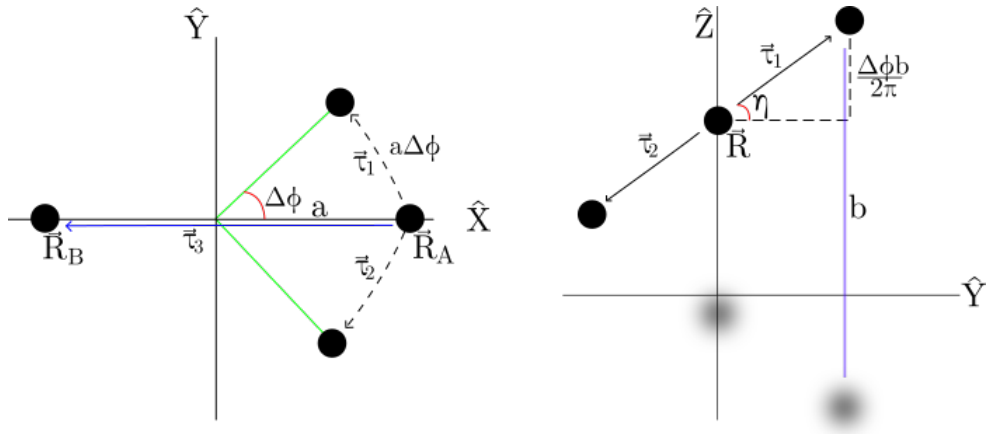

Figure 3.2: A detailed view of the unit vectors connecting the sites in the structure model of DNA with the fix basis axis. From this image, the 3 connecting vectors can be deduced and these are defined in Eq. 3.1 in the rotating basis. The amount of bases per turn in the model is actually 10 not 6; this was drawn to ease the identification of b as the pitch. The component in $\hat{y}$ of τ_1 the arc resulting from the radius, a, multiplied by the angle between sites, $\Delta\phi$. The component in $\hat{z}$ of τ_1 is the pitch, b, multiplied by the angle between each site, $\Delta\phi$, divided by 2π. τ_3 has only a component in $\hat{x}$ which is $-2a$.

The base or unit vectors are described in figure 3.2. Here, $\tau_{1,2}^{A,B}$ are the intra-helix unit vectors and τ_3 is the inter-helix unit vector. The definitions of the vectors in the local coordinate system of the basis A and B are:

$$\tau_1^{A,B} = a\Delta\phi\hat{y} + \frac{b\Delta\phi}{2\pi}\hat{z}, \quad \tau_2^{A,B} = -a\Delta\phi\hat{y} - \frac{b\Delta\phi}{2\pi}\hat{z}, \quad \tau_3 = -2a\hat{x}. \tag{3.1}$$

In a helix with the sites starting onto the $\hat{X}$ axis, the coordinates of the base, $\mathbf{R}_I^i$, where $i = 0, 1, 2, \cdots N$ and $I = A, B$, are given by:

$$\mathbf{R}_I^i = a\cos[i\Delta\phi]\hat{X} + a\sin[i\Delta\phi]\hat{Y} + \frac{ib\Delta\phi}{2\pi}\hat{Z},$$

where the A site starts at the positive end of $\hat{X}$ and site B starts at the opposite end (signs for the first two terms change to negative). Now, with considering this structure, the model for the electron-phonon interaction in DNA is presented in the next section.

3.2 Electron-phonon interaction in DNA

The nearest neighbor tight-binding model was build by considering the hoppings between neighboring sites as a linear combination of their wavefunctions, with the coefficients being the hopping integrals, t. The value of these coefficients is given in terms of Slater and Koster parameters, explained in section 2.2. By considering spinless electrons in the structure previously described, the model is given by the equations:

$$\epsilon\Psi_A(\mathbf{R}_A) = \sum_{l=1}^{2} t^{in}_{\mathbf{R}_A,\mathbf{R}_A+\tau_l^A}\Psi_A(\mathbf{R}_A+\tau_l^A) + t^{out}_{\mathbf{R}_A,\mathbf{R}_A+\tau_3}\Psi_B(\mathbf{R}_A+\tau_3), \tag{3.2}$$

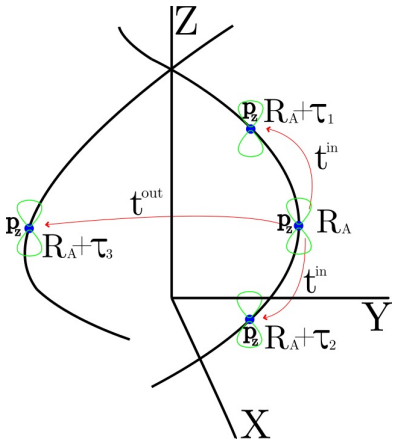

Figure 3.3: Graphical description of the electron-phonon model. There are three couplings to first neighbors with each one corresponding to a translation of each base vector with an associated amplitude. The intra-helix couplings have amplitudes t^{in} and inter-helix has t^{out}.

and:

$$\epsilon\Psi_B(\mathbf{R}_B) = \sum_{l=1}^{2} t^{in}_{\mathbf{R}_B,\mathbf{R}_B+\tau_l^B}\Psi_B(\mathbf{R}_B+\tau_l^B) + t^{out}_{\mathbf{R}_B,\mathbf{R}_B-\tau_3}\Psi_A(\mathbf{R}_B-\tau_3), \tag{3.3}$$

where the first equation is described in figure 3.3; here, the first term describes the overlap between wavefunctions on $\mathbf{R}_A$ and $\mathbf{R}_A+\tau_l$ sites (intra helix), and the second term describes the overlap between $\mathbf{R}_A$ and $\mathbf{R}_A+\tau_3$ sites (inter helix); the description is similar for the second equation. In these equations, ϵ is the eigenvalue of the corresponding Schrödinger equation, $\Psi_{A,B}$ are the wavefunctions defined in Eq. 2.14 and Eq. 2.15; and $t^{in,out}_{\mathbf{R}_I,\mathbf{R}_{I'}-\tau_l^{I'}}$ is the hopping integral coupling between sites $I = A, B$. Super-indexes *in* and *out* refer to intra-helix ($A \to A$ or $B \to B$) and inter-helix ($A \to B$) coupling respectively.

The envelope function approximation was used to define the wavefunctions in Eq. 2.14 and Eq. 2.15. These functions are constructed as the sum of two plane waves multiplied by the envelope function at the symmetry points in the first Brillouin zone at the Fermi level: $\mathbf{K} = \frac{\pi}{2R^2}(0, a\Delta\phi, \frac{b\Delta\phi}{2\pi})$ and $\mathbf{K}' = -\mathbf{K}$. The wavefunctions were simplified as:

$$\Psi_A(\mathbf{R}_A) = \mathcal{A}^\dagger(\mathbf{R}_A)F_A(\mathbf{R}_A), \quad \Psi_B(\mathbf{R}_B) = \mathcal{B}^\dagger(\mathbf{R}_B)F_B(\mathbf{R}_B), \tag{3.4}$$

by defining the auxiliary vectors:

$$\mathcal{A}^\dagger(\mathbf{R}_A) = \begin{pmatrix} e^{i\mathbf{K}\cdot\mathbf{R}_A} & e^{i\mathbf{K}'\cdot\mathbf{R}_A} \end{pmatrix}, \quad \mathcal{B}^\dagger(\mathbf{R}_B) = \begin{pmatrix} e^{i\mathbf{K}\cdot\mathbf{R}_B} & e^{i\mathbf{K}'\cdot\mathbf{R}_B} \end{pmatrix},$$

and:

$$F_I(\mathbf{R}_I) = \begin{pmatrix} F_I^{\mathbf{K}}(\mathbf{R}_I) \\ F_I^{\mathbf{K}'}(\mathbf{R}_I) \end{pmatrix},$$

with $I = A, B$.

The TB model equations were solved separately, starting with the TB equation for A sites. First, Eq. 3.2, is multiplied by $\mathcal{A}(\mathbf{R}_A)$ and $\sum_{\mathbf{R}_A} g(\mathbf{r}-\mathbf{R}_A)$, where $g(\mathbf{r}-\mathbf{R}_A)$ is the smoothing function. This function has properties that include changing smoothly for $|\mathbf{r}| < |\mathbf{R}_A|$, decaying fast for $|\mathbf{r}| > |\mathbf{R}_A|$, and the sum $\sum_{\mathbf{R}_A} g(\mathbf{r}-\mathbf{R}_A) = 1$[62]; in this case, $\mathbf{r}$ is the magnitude of the unit vectors. This function was used to smear out the point

functions as: $y(\mathbf{R}) \rightarrow y(\mathbf{r})$. After the operations, Eq. 3.4 is substituted to obtain:

$$\begin{aligned}\mathcal{A}(\mathbf{R}_A)\epsilon\mathcal{A}^\dagger(\mathbf{R}_A)F_A(\mathbf{R}_A)\sum_{\mathbf{R}_A} g(\mathbf{r}-\mathbf{R}_A) = \mathcal{A}(\mathbf{R}_A)\Bigg(\sum_{l=1}^{2} t^{in}_{\mathbf{R}_A,\mathbf{R}_A+\tau_l^A}\mathcal{A}^\dagger(\mathbf{R}_A+\tau_l^A) \\ \times F_A(\mathbf{R}_A+\tau_l^A) + t^{out}_{\mathbf{R}_A,\mathbf{R}_A+\tau_3}\mathcal{B}^\dagger(\mathbf{R}_A+\tau_3)F_B(\mathbf{R}_B)\Bigg)\sum_{\mathbf{R}_A} g(\mathbf{r}-\mathbf{R}_A).\end{aligned} \tag{3.5}$$

Here, $\mathcal{A}(\mathbf{R}_A)\mathcal{A}^\dagger(\mathbf{R}_A) = \mathbb{1}$ is the 2×2 unit matrix, and the matrix products $\mathcal{A}(\mathbf{R}_A)\mathcal{A}^\dagger(\mathbf{R}_A+\tau_\mathbf{l}^\mathbf{A})$ and $\mathcal{A}(\mathbf{R}_A)\mathcal{B}^\dagger(\mathbf{R}_A+\tau_\mathbf{3})$ result in:

$$\mathcal{A}(\mathbf{R}_A)\mathcal{A}^\dagger(\mathbf{R}_A+\tau_l^A) = \begin{pmatrix} e^{i\mathbf{K}\cdot\tau_l^A} & 0 \\ 0 & e^{i\mathbf{K}'\cdot\tau_l^A}\end{pmatrix}, \mathcal{A}(\mathbf{R}_A)\mathcal{B}^\dagger(\mathbf{R}_A+\tau_3) = \begin{pmatrix} e^{i\mathbf{K}\cdot\tau_3} & 0 \\ 0 & e^{i\mathbf{K}'\cdot\tau_3}\end{pmatrix}. \tag{3.6}$$

The smoothing function was used to transform $F_I(\mathbf{R})$ into $F_I(\mathbf{r})$; and a second order Taylor series was performed around $\mathbf{r}$ to obtain: $F_I(\mathbf{r}+\tau) \approx F_I(\mathbf{r}) + \tau\cdot\nabla F_I(\mathbf{r})$. The series was done until second order since the third and upcoming terms include powers of the lattice vectors that exponentially reduce their relevance in the results.

Phonons in this system were included due to a modulation in the transfer integral (as has been done for nanotubes[76, 77]) by using the equation:

$$t^{in,out}_{\mathbf{R}_I,\mathbf{R}_I+\tau_l^I} = t_o^{in,out} - \frac{\beta^{in,out}t_o^{in,out}}{c^2}\tau_l^{I'}\cdot[\mathbf{u}_I(\mathbf{R}_I) - \mathbf{u}_{I'}(\mathbf{R}_I+\tau_l^I)], \tag{3.7}$$

where the first term is the transfer integral without perturbation and the second term is the perturbation produced due to phonons. This perturbation was modeled by the differences in lattice displacements of the sites multiplied by a coefficient that quantifies the change in the transfer integral with such movement. The parameter, $c = |\tau_l^I|$ is the distance between sites, $\mathbf{u}_I(\mathbf{R}_I)$ is the lattice displacement of A and B sites, and $\beta^{in,out}$ is defined as:

$$\beta^{in,out} = -\frac{c}{t_0^{in,out}}\frac{\partial}{\partial c}t_0^{in,out}.$$

From solid state physics, phonons are divided into acoustic and optical. This separation was included by defining acoustic, $\mathbf{u}$, and optical, $\mathbf{v}$, amplitudes:

$$\mathbf{u}(\mathbf{R}) \approx \frac{1}{\sqrt{2}}(\mathbf{u}_I(\mathbf{R}) + \mathbf{u}_{I'}(\mathbf{R})), \qquad \mathbf{v}(\mathbf{R}) \approx \frac{1}{\sqrt{2}}(\mathbf{u}_I(\mathbf{R}) - \mathbf{u}_{I'}(\mathbf{R})). \tag{3.8}$$

Expressions for the continuous lattice displacement were obtained by using the smoothing function: $\mathbf{u}_I(\mathbf{R}) \rightarrow \mathbf{u}_I(\mathbf{r})$; performing the Taylor series expansion around $\mathbf{r}$ (up to second order since little vibrations are considered and further terms are too small), and using Eq. (3.8). This lead to:

$$\mathbf{u}_A(\mathbf{R}_A) - \mathbf{u}_A(\mathbf{R}_A+\tau_l^A) \approx -(\tau_l^A\cdot\nabla)(\alpha^{ac}\mathbf{u}(\mathbf{r}) + \alpha^{op}\mathbf{v}(\mathbf{r})), \tag{3.9}$$

and:

$$\mathbf{u}_A(\mathbf{R}_A) - \mathbf{u}_B(\mathbf{R}_A+\tau_3) \approx -(\tau_3\cdot\nabla)(\alpha^{ac}\mathbf{u}(\mathbf{r}) - \alpha^{op}\mathbf{v}(\mathbf{r})) + 2\alpha^{op}\mathbf{v}(\mathbf{r}), \tag{3.10}$$

which were substituted into the expression for the electron-phonon interaction (Eq. 3.7). The effect of each amplitude was parametrized by substituting $\frac{1}{\sqrt{2}} = \alpha^{ac,op}$, a constant

that can be used to control the electron-phonon interaction independently for acoustic or optical phonons.

Now Eq. 3.6, Eq. 3.7, Eq. 3.9 and Eq. 3.10 were substituted into Eq. 3.5 to get:

$$\begin{aligned}
&\epsilon F_A(\mathbf{r}) \sum_{\mathbf{R}_A} g(\mathbf{r}-\mathbf{R}_A)\mathbb{1} = \\
&\left(\sum_{l=1}^{2}\left(t_o^{in} + \frac{\beta^{in} t_o^{in}}{c^2}\tau_l^A \cdot [(\tau_l^A \cdot \nabla)(\alpha^{ac}\mathbf{u}(\mathbf{r}) + \alpha^{op}\mathbf{v}(\mathbf{r}))]\right)\right. \\
&\begin{pmatrix} e^{i\mathbf{K}\cdot\tau_l^A} & 0 \\ 0 & e^{i\mathbf{K}'\cdot\tau_l^A}\end{pmatrix}\Big(F_A(\mathbf{r}) + \tau_l^A \cdot \nabla F_A(\mathbf{r})\Big) \\
&+\left(t_o^{out} + \frac{\beta^{out} t_o^{out}}{c^2}\tau_3 \cdot [(\tau_3 \cdot \nabla)(\alpha^{ac}\mathbf{u}(\mathbf{r}) - \alpha^{op}\mathbf{v}(\mathbf{r})) - 2\alpha^{op}\mathbf{v}(\mathbf{r})]\right) \\
&\left.\begin{pmatrix} e^{i\mathbf{K}\cdot\tau_3} & 0 \\ 0 & e^{i\mathbf{K}'\cdot\tau_3}\end{pmatrix}\Big(F_B(\mathbf{r}) + \tau_3 \cdot \nabla F_B(\mathbf{r})\Big)\right)\sum_{\mathbf{R}_A} g(\mathbf{r}-\mathbf{R}_A).
\end{aligned} \tag{3.11}$$

Then, since nothing else depends on $\mathbf{R}_A$, the sum $\sum_{\mathbf{R}_A} g(\mathbf{r}-\mathbf{R}_A)$ was substituted by 1.

It will be useful to know these products for the incoming calculations:

$$\begin{aligned}
\mathbf{K}\cdot\tau_1^A &= (\frac{\pi}{2R}\hat{y} + \frac{\pi}{2R}\tan(\eta)\hat{z})(a\Delta\phi\hat{y} + \frac{b\Delta\phi}{2\pi}\hat{z}) \\
&= a\Delta\phi\frac{\pi}{2R} + \frac{b\Delta\phi}{2\pi}\frac{\pi}{2R}tan(\eta) = a\Delta\phi\frac{\pi}{2R} + \frac{b^2\Delta\phi}{8\pi aR} \\
&= \frac{\pi}{2R}(a\Delta\phi + \frac{b^2\Delta\phi}{4\pi^2 a}) = \frac{\pi}{2R}R = \frac{\pi}{2}, \\
\mathbf{K}\cdot\tau_2^A &= -\frac{\pi}{2}, \quad \mathbf{K}\cdot\tau_3 = 0.
\end{aligned} \tag{3.12}$$

By taking up to second order terms in τ_l^A and τ_3 in Eq. (3.11), each term has three other terms. The first three terms are intra-helix and the rest are inter-helix. These were treated and analyzed separately:

- **1st term.** This is the intra-helix term without phonon interaction, or kinetic term, multiplied by the first term of the Taylor series expansion of the envelope function. Then this could be called the kinetic intra-helix first order term. This term vanished since the result was:

$$\begin{aligned}
\sum_{l=1}^{2} t_o^{in}\begin{pmatrix} e^{i\mathbf{K}\cdot\tau_l^A} & 0 \\ 0 & e^{i\mathbf{K}'\cdot\tau_l^A}\end{pmatrix}F_A(\mathbf{r}) &= t_o^{in}\begin{pmatrix} \sum_{l=1}^{2} e^{i\mathbf{K}\cdot\tau_l^A} & 0 \\ 0 & \sum_{l=1}^{2} e^{i\mathbf{K}'\cdot\tau_l^A}\end{pmatrix}F_A(\mathbf{r}) \\
&= 0,
\end{aligned} \tag{3.13}$$

  because the sums resulted in:

$$\sum_{l=1}^{2} e^{i\mathbf{K}\cdot\tau_l^A} = e^{i\frac{\pi}{2}} + e^{-i\frac{\pi}{2}} = 2\cos\left(\frac{\pi}{2}\right) = 0, \quad \sum_{l=1}^{2} e^{i\mathbf{K}'\cdot\tau_l^A} = 0.$$

  The meaning for the disappearance of this term relies on the result of the sum: $2\cos(\pi/2)$, where the argument of cos is given by Eq. 3.12. In the symmetry the

points, the greatest contribution of the kinetic term of the intra-helix coupling vanishes, thus the intra-helix kinetic ET has a lower relevance. Nevertheless, in points different than the symmetry, this contribution reemerges and increases further away from these points up to half or twice their position.

- **2nd term.** This is the second order intra-helix kinetic term because it contains the second term of the envelope function's Taylor expansion. This is numerically much smaller than the first one since it is multiplied by base vectors with units in Å range. The calculations were:

$$\begin{aligned}&\sum_{l=1}^{2} t_o^{in} \begin{pmatrix} e^{i\mathbf{K}\cdot\tau_l^A} & 0 \\ 0 & e^{i\mathbf{K}'\cdot\tau_l^A} \end{pmatrix} \tau_l^A \cdot \nabla F_A(\mathbf{r}) = \\ &t_o^{in} \begin{pmatrix} \sum_{l=1}^{2} e^{i\mathbf{K}\cdot\tau_l^A}\tau_l^A & 0 \\ 0 & \sum_{l=1}^{2} e^{i\mathbf{K}'\cdot\tau_l^A}\tau_l^A \end{pmatrix} \cdot \nabla F_A(\mathbf{r}),\end{aligned} \tag{3.14}$$

where the sums gave:

$$\begin{aligned}\sum_{l=1}^{2} e^{i\mathbf{K}\cdot\tau_l^A}\tau_l^A &= e^{i\frac{\pi}{2}}(a\Delta\phi\hat{\mathrm{y}} + \frac{b\Delta\phi}{2\pi}\hat{\mathrm{z}}) - e^{-i\frac{\pi}{2}}(a\Delta\phi\hat{\mathrm{y}} + \frac{b\Delta\phi}{2\pi}\hat{\mathrm{z}}) \\ &= 2i(a\Delta\phi\hat{\mathrm{y}} + \frac{b\Delta\phi}{2\pi}\hat{\mathrm{z}})\sin\left(\frac{\pi}{2}\right) \\ &= 2i(a\Delta\phi\hat{\mathrm{y}} + \frac{b\Delta\phi}{2\pi}\hat{\mathrm{z}}), \\ \sum_{l=1}^{2} e^{i\mathbf{K}'\cdot\tau_l^A}\tau_l^A &= -2i(a\Delta\phi\hat{\mathrm{y}} + \frac{b\Delta\phi}{2\pi}\hat{\mathrm{z}}).\end{aligned}$$

Then Eq. 3.14 resulted in:

$$t_o^{in} \begin{pmatrix} 2i(a\Delta\phi\hat{\mathrm{y}} + \frac{b\Delta\phi}{2\pi}\hat{\mathrm{z}}) & 0 \\ 0 & -2i(a\Delta\phi\hat{\mathrm{y}} + \frac{b\Delta\phi}{2\pi}\hat{\mathrm{z}}) \end{pmatrix} \cdot \nabla F_A(\mathbf{r}).$$

Here, the definition of the momentum operator, $\hat{\mathbf{p}} = -i\hbar\nabla$, was used to obtain $\nabla = i\hat{\mathbf{p}}/\hbar$, which gave $\nabla = i\mathbf{k}$, where $\mathbf{k} = k_x\hat{x} + k_y\hat{y} + k_z\hat{z}$ so $\nabla = i(k_x\hat{x} + k_y\hat{y} + k_z\hat{z})$, and by substituting this into the previous equation it was obtained:

$$t_o^{in} \begin{pmatrix} -2(a\Delta\phi k_y + \frac{b\Delta\phi}{2\pi}k_z) & 0 \\ 0 & 2(a\Delta\phi k_y + \frac{b\Delta\phi}{2\pi}k_z) \end{pmatrix} F_A(\mathbf{r}).$$

Then, the relations: $k_z = k_y \tan\eta = k_y b/(2\pi a)$ and $a\Delta\phi + (b^2\Delta\phi/(4\pi^2 a)) = R$, were used to obtain:

$$\begin{aligned}&- t_o^{in} \begin{pmatrix} 2(a\Delta\phi + \frac{b\Delta\phi}{2\pi}\tan\eta)k_y & 0 \\ 0 & -2(a\Delta\phi + \frac{b\Delta\phi}{2\pi}\tan\eta)k_y \end{pmatrix} F_A(\mathbf{r}) \\ &= -t_o^{in} 2R\nu k_y F_A(\mathbf{r}),\end{aligned} \tag{3.15}$$

where ν is $+1$ for $\mathbf{K}$ and -1 for $\mathbf{K}'$. The change of sign of this result with $\mathbf{K}$ is directly related with the change of sign of $\mathbf{K}$ and $\mathbf{K}'$. This means that there is a second order contribution of the kinetic term in the intra-helix ET of DNA that keeps this coupling from completely vanishing at the symmetry points.

- **3rd term.** This is the electron-phonon intra-helix term. Only the first order Envelope functions' Taylor expansions were considered since the unit vectors are already at second order and further orders greatly decrease the relevance of such terms. The calculations were done as follows:

$$\begin{aligned}&\sum_{l=1}^{2}\frac{\beta^{in}t_o^{in}}{c^2}\tau_l^A\cdot[(\tau_l^A\cdot\nabla)(\alpha^{ac}\mathbf{u}(\mathbf{r})+\alpha^{op}\mathbf{v}(\mathbf{r}))]\begin{pmatrix}e^{i\mathbf{K}\cdot\tau_l^A} & 0\\ 0 & e^{i\mathbf{K}'\cdot\tau_l^A}\end{pmatrix}F_A(\mathbf{r})=\\&\frac{\beta^{in}t_o^{in}}{c^2}\begin{pmatrix}\sum_{l=1}^{2}e^{i\mathbf{K}\cdot\tau_l^A}\tau_l^A(\tau_l^A\cdot\nabla) & 0\\ 0 & \sum_{l=1}^{2}e^{i\mathbf{K}'\tau_l^A}\tau_l^A\cdot(\tau_l^A\cdot\nabla)\end{pmatrix}\\&\cdot(\alpha^{ac}\mathbf{u}(\mathbf{r})+\alpha^{op}\mathbf{v}(\mathbf{r}))F_A(\mathbf{r}),\end{aligned}\tag{3.16}$$

where the sums resulted in:

$$\begin{aligned}&\sum_{l=1}^{2}e^{i\mathbf{K}\cdot\tau_l^A}\tau_l^A(\tau_l^A\cdot\nabla)=e^{i\frac{\pi}{2}}(a\Delta\phi\hat{\mathrm{y}}+\frac{b\Delta\phi}{2\pi}\hat{\mathrm{z}})(a\Delta\phi\partial_y+\frac{b\Delta\phi}{2\pi}\partial_z)\\&+e^{-i\frac{\pi}{2}}(-a\Delta\phi\hat{\mathrm{y}}-\frac{b\Delta\phi}{2\pi}\hat{\mathrm{z}})(-a\Delta\phi\partial_y-\frac{b\Delta\phi}{2\pi}\partial_z)\\&=(a\Delta\phi\hat{\mathrm{y}}+\frac{b\Delta\phi}{2\pi}\hat{\mathrm{z}})(a\Delta\phi\partial_y+\frac{b\Delta\phi}{2\pi}\partial_z)2\cos\left(\frac{\pi}{2}\right)=0,\\&\sum_{l=1}^{2}e^{i\mathbf{K}'\cdot\tau_l^A}\tau_l^A(\tau_l^A\cdot\nabla)=0,\end{aligned}$$

so Eq. 3.16 ended up as:

$$\frac{\beta^{in}t_o^{in}}{c^2}\begin{pmatrix}0 & 0\\ 0 & 0\end{pmatrix}\cdot(\alpha^{ac}\mathbf{u}(\mathbf{r})+\alpha^{op}\mathbf{v}(\mathbf{r}))F_A(\mathbf{r})=0.\tag{3.17}$$

Therefore the electron-phonon interaction vanishes for the intra-helix ET, thus this process is achieved without phonon intervention at first order in the symmetry points. The cause of the vanishing of this term is the same as for the 1st term. Now the terms for the inter-helix ET are derived.

- **4th term** This term is the first order kinetic contribution to inter-helix ET. The term resulted in:

$$t_o^{out}\begin{pmatrix}e^{i\mathbf{K}\cdot\tau_3} & 0\\ 0 & e^{i\mathbf{K}'\cdot\tau_3}\end{pmatrix}F_B(\mathbf{r})=t_o^{out}\mathbb{1}F_B(\mathbf{r}).\tag{3.18}$$

Then, inter-helix ET contains the first order kinetic term with only the t_o^{out} amplitude as coefficient. It can be observed that the change in sign for different $\mathbf{K}$ does not occur. This is because in the inter-helix coupling is on a different plane than the symmetry points, so the base vector τ_3 doesn't have components in the $\hat{y}$ or $\hat{z}$ directions, therefore only a 2×2 unit matrix, $\mathbb{1}$, is obtained; and the energy is independent of which symmetry point is chosen. This last consequence repeated on the following two terms.

- **5th term** This is the second order kinetic term in the inter-helix regime. The calculations were:

$$\begin{aligned}&t_o^{out}\begin{pmatrix}e^{i\mathbf{K}\cdot\tau_3} & 0\\ 0 & e^{i\mathbf{K}'\cdot\tau_3}\end{pmatrix}\tau_3\cdot\nabla F_B(\mathbf{r})=t_o^{out}\begin{pmatrix}e^{i\mathbf{K}\cdot\tau_3}\tau_3 & 0\\ 0 & e^{i\mathbf{K}'\cdot\tau_3}\tau_3\end{pmatrix}\cdot\nabla F_B(\mathbf{r})\\&=t_o^{out}\begin{pmatrix}-2a\hat{\mathrm{x}} & 0\\ 0 & -2a\hat{\mathrm{x}}\end{pmatrix}\cdot\nabla F_B(\mathbf{r})=-t_o^{out}2aik_x\mathbb{1}F_B(\mathbf{r}).\end{aligned}\tag{3.19}$$

Therefore, inter-helix ET also contains second order kinetic terms. This term contains the imaginary unit, i, arising from the Del operator, ∇, of the second order Taylor expansion of the envelope function.

- **6th term** The inter-helix term with electron-phonon interaction gave:

$$\frac{\beta^{out}t_o^{out}}{c^2}\tau_3\cdot[(\tau_3\cdot\nabla)(\alpha^{ac}\mathbf{u}(\mathbf{r})-\alpha^{op}\mathbf{v}(\mathbf{r}))-2\alpha^{op}\mathbf{v}(\mathbf{r})]\begin{pmatrix}e^{i\mathbf{K}\cdot\tau_3} & 0\\ 0 & e^{i\mathbf{K}'\cdot\tau_3}\end{pmatrix}F_B(\mathbf{r})$$
$$=\frac{\beta^{out}t_o^{out}}{c^2}\Bigg[\begin{pmatrix}e^{i\mathbf{K}\cdot\tau_3}\tau_3(\tau_3\cdot\nabla) & 0\\ 0 & e^{i\mathbf{K}'\tau_3}\tau_3(\tau_3\cdot\nabla)\end{pmatrix}\cdot(\alpha^{ac}\mathbf{u}(\mathbf{r})-\alpha^{op}\mathbf{v}(\mathbf{r}))$$
$$-\begin{pmatrix}e^{i\mathbf{K}\cdot\tau_3}\tau_3 & 0\\ 0 & e^{i\mathbf{K}'\cdot\tau_3}\tau_3\end{pmatrix}\cdot 2\alpha^{op}\mathbf{v}(\mathbf{r})\Bigg]F_B(\mathbf{r}),$$

where $\tau_3\cdot\nabla=-2a\partial_x$, so $\tau_3\cdot(\tau_3\cdot\nabla)=4a^2\partial_x\hat{\mathrm{x}}$. Then this term became:

$$\frac{\beta^{out}t_o^{out}}{c^2}\Bigg[\begin{pmatrix}4a^2\partial_x\hat{\mathrm{x}} & 0\\ 0 & 4a^2\partial_x\hat{\mathrm{x}}\end{pmatrix}\cdot(\alpha^{ac}\mathbf{u}(\mathbf{r})-\alpha^{op}\mathbf{v}(\mathbf{r}))$$
$$-\begin{pmatrix}-2a\hat{\mathrm{x}} & 0\\ 0 & -2a\hat{\mathrm{x}}\end{pmatrix}\cdot 2\alpha^{op}\mathbf{v}(\mathbf{r})\Bigg]F_B(\mathbf{r}), \tag{3.20}$$

and by using the definition of acoustic and optic amplitudes ($\mathbf{u}(\mathbf{r})=u_x\hat{\mathrm{x}}+u_y\hat{\mathrm{y}}+u_z\hat{\mathrm{z}}$ and $\mathbf{v}(\mathbf{r})=v_x\hat{\mathrm{x}}+v_y\hat{\mathrm{y}}+v_z\hat{\mathrm{z}}$, respectively) in Eq. 3.20 it was obtained:

$$\frac{\beta^{out}t_o^{out}}{c^2}\Bigg[\begin{pmatrix}4a^2\partial_x(\alpha^{ac}u_x-\alpha^{op}v_x) & 0\\ 0 & 4a^2\partial_x(\alpha^{ac}u_x-\alpha^{op}v_x)\end{pmatrix}$$
$$-\begin{pmatrix}-4a\alpha^{op}v_x & 0\\ 0 & -4a\alpha^{op}v_x\end{pmatrix}\Bigg]F_B(\mathbf{r}) \tag{3.21}$$
$$=\frac{4\beta^{out}t_o^{out}}{c^2}(a^2\partial_x(\alpha^{ac}u_x-\alpha^{op}v_x)+a\alpha^{op}v_x)\mathbb{1}F_B(\mathbf{r}).$$

Therefore inter-helix ET is also affected by the phonon presence. It can be observed that acoustical phonons are multiplied to the second order term, a^2, which is the helix radius, while the optical phonons contain, in addition to the second order, a first order term. This means that optical phonons will have more impact on the ET in DNA.

By adding together all the terms from Eqs. (3.13) to (3.21), into Eq. (3.11), resulted in:

$$\epsilon F_A(\mathbf{r})\mathbb{1}=-t_o^{in}2R\nu k_yF_A(\mathbf{r})$$
$$+t_o^{out}\big(1-2aik_x+\frac{4\beta^{out}}{c^2}(a^2\partial_x(\alpha^{ac}u_x-\alpha^{op}v_x)+a\alpha^{op}v_x)\big)\mathbb{1}F_B(\mathbf{r}),$$

which is the final equation resulting from Eq. 3.2. Here, the influence of the terms in the model can be observed and compared. The intra-helix ET depends only in the second order kinetic term while the inter-helix contains all terms considered. A similar procedure for the model of B sites was followed and the result was:

$$\epsilon F_B(\mathbf{r})\mathbb{1}=-t_o^{in}2R\nu k_yF_B(\mathbf{r})$$
$$+t_o^{out}\big(1+2aik_x+\frac{4\beta^{out}}{c^2}(a^2\partial_x(\alpha^{ac}u_x-\alpha^{op}v_x)+a\alpha^{op}v_x)\big)\mathbb{1}F_A(\mathbf{r}),$$

which is very similar to the other one but two signs change. The first is the sign associated with the imaginary unit, i, and the second is the sign on the sum of the second order phonon amplitudes. The behavior of the ET remains the same as for A sites so the intra-helix contains only the second order kinetic term while inter-helix is driven by both phonon and kinetic interactions.

Now, by defining the parameter: $\gamma^{out} = 1 - 2aik_x + \frac{4\beta^{out}}{c^2}(a^2\partial_x(\alpha^{ac}u_x - \alpha^{op}v_x) + a\alpha^{op}v_x)$; the full Schrödinger equation can be written as:

$$\mathcal{H}\mathbf{F}(\mathbf{r}) = \varepsilon\mathbf{F}(\mathbf{r}), \tag{3.22}$$

with:

$$\mathcal{H} = \begin{pmatrix} \mathcal{H}^{\mathbf{K}} & \mathbf{0} \\ \mathbf{0} & \mathcal{H}^{\mathbf{K}'} \end{pmatrix}, \qquad \mathbf{F}(\mathbf{r}) = (\mathbf{F}^{\mathbf{K}}(\mathbf{r}), \mathbf{F}^{\mathbf{K}'}(\mathbf{r})); \tag{3.23}$$

where: $\mathbf{F}^{\mathbf{K}^{(\prime)}}(\mathbf{r}) = (\mathbf{F}_A^{\mathbf{K}^{(\prime)}}(\mathbf{r}), \mathbf{F}_B^{\mathbf{K}^{(\prime)}}(\mathbf{r}))$, and:

$$\mathcal{H}^{\mathbf{K},\mathbf{K}'} = \begin{pmatrix} -t_o^{in} 2R\nu k_y & t_o^{out}\gamma^{out} \\ t_o^{out}\gamma^{out\dagger} & -t_o^{in} 2R\nu k_y \end{pmatrix}; \tag{3.24}$$

here, $\nu = +1$ for $\mathbf{K}$ and $\nu = -1$ for $\mathbf{K}'$. The values for a, b, and $\Delta\phi$ in this model are 1.19 nm, 3.4 nm and $2\pi/10 = \pi/5$. The values of the remaining parameters were obtained from Peralta[62]: $t_o^{in} = -10$ meV $= t_o^{out}$, $c = 0.89$ nm (intra-helix), $c = 2.37$ nm (inter-helix), $\beta^{in} \approx 2.7$, $\beta^{out} \approx 2.2$. These values were consistent with the results from Kalosakas[89], and it was found that decoherence effects can be modulated by this coupling.

In comparison with the results from Solmar et al. in Eq. 2.10, their kinetic intra-helix term obtained: $-2\nu q_y R t^{in}\mathbf{1}_{\sigma'}\mathbf{1}_s$, is identical to the one obtained: $-t_o^{in}2R\nu k_y$. This is expected since both approaches only consider the $p_z - p_z$ coupling and the same structure, and this agreement further validates the approach presented. Their inter-helix term: $t^{out}{\sigma'}_x\mathbf{1}_s$, differs from the derived: $t_o^{out}\gamma_A$. The extra parameters, $\gamma_{A,B}$, appear due to the electron-phonon interaction as an additional coefficient that modulates the helix to helix coupling. The other terms will be discussed in the next section because they include the spin effect.

Regarding this interaction, it has been observed in the obtained Hamiltonian that phonons are relevant only in the inter-helix ET as the modulation only appears in this regime. This is caused by the symmetry points being defined in different axis directions than the inter-helix base vector, τ_3. The intra-helix contribution of phonons disappears due to the base vectors being opposite to each other, which is the result of the structure model and the rotating basis.

Also, phonons were divided in optical and acoustical modes which interacted in a different way in the model since optical modes appear at first order while acoustical only appear at second order; thus the optical phonons have more relevance in this process and since coherence is affected by phonons[62], the second order contribution can explain the large coherence lengths observed experimentally[26].

The ability to reproduce results makes this methodology an important to consider when approaching an ET problem in studies with this type of molecules. As reviewed, spintronics is one interested in this subject, but these are more interested in the effect of spin rather than phonons; so in the next section the effect of spin is implemented to compare the results and observe what implications arise from this new factor.

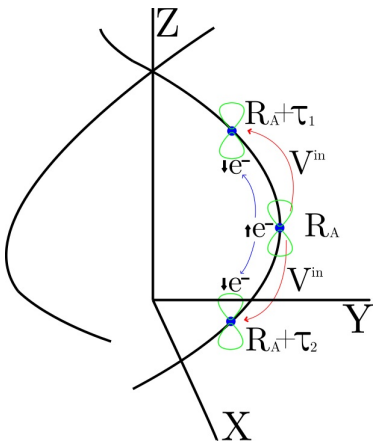

Figure 3.4: Graphical description of the addition of the intrinsic SO effect. There are two additional couplings to first neighbors with each one corresponding to a translation of each intra-helix base vector with an associated amplitude V^{in}.

3.3 Spin-phonon interaction in DNA

To include spin-orbit the interaction, the TB model introduced in Eq. 3.2 and Eq. 3.3 was adapted by considering the intrinsic spin-orbit (SO) coupling. This was included with amplitude: $V_o^{in} = \lambda_{SO}^{in}\nu_l$, defined by Varela[81], where $\nu_l = +1$ for $l = 1$ and $\nu_l = -1$ for $l = 2$. In this amplitude, λ_{SO}^{in} represents the intrinsic spin-orbit coupling.

The hopping integrals are build based on Slater and Koster parameters, the modulation due to phonons and the intrinsic SO effect. This coupling is described in figure 3.4, where the p_z orbital is coupled to the p_x or p_y orbitals of the same site, and overlaps the last orbital to the p_z orbital of another site, with a spin-flip occurring in the last step. The inter-helix term is only dependent on Rashba coupling which is considered to be non existent in this case. Taking these considerations, the model proposed adds the intra-helix coupling term and the spin effect as:

$$\begin{aligned}\varepsilon\Psi_{A\uparrow/\downarrow}(\mathbf{R}_A) &= \sum_{l=1}^{2} t^{in}_{\mathbf{R}_{A\uparrow/\downarrow},(\mathbf{R}_A+\tau_l^A)_{\uparrow/\downarrow}}\Psi_{A\uparrow/\downarrow}(\mathbf{R}_A+\tau_l^A) \\ &+ \sum_{l=1}^{2} V^{in}_{\mathbf{R}_{A\uparrow/\downarrow},(\mathbf{R}_A+\tau_l^A)_{\downarrow/\uparrow}}\Psi_{A\downarrow/\uparrow}(\mathbf{R}_A+\tau_l^A) + t^{out}_{\mathbf{R}_{A\uparrow/\downarrow},(\mathbf{R}_A+\tau_3)_{\uparrow/\downarrow}}\Psi_{B\uparrow/\downarrow}(\mathbf{R}_A+\tau_3),\end{aligned} \tag{3.25}$$

$$\begin{aligned}\varepsilon\Psi_{B\uparrow/\downarrow}(\mathbf{R}_B) &= \sum_{l=1}^{2} t^{in}_{\mathbf{R}_{B\uparrow/\downarrow},(\mathbf{R}_B+\tau_l^B)_{\uparrow/\downarrow}}\Psi_{B\uparrow/\downarrow}(\mathbf{R}_B+\tau_l^B) \\ &+ \sum_{l=1}^{2} V^{in}_{\mathbf{R}_{B\uparrow/\downarrow},(\mathbf{R}_B+\tau_l^B)_{\downarrow/\uparrow}}\Psi_{B\downarrow/\uparrow}(\mathbf{R}_B+\tau_l^B) + t^{out}_{\mathbf{R}_{B\uparrow/\downarrow},(\mathbf{R}_B-\tau_3)_{\uparrow/\downarrow}}\Psi_{A\uparrow/\downarrow}(\mathbf{R}_B-\tau_3),\end{aligned} \tag{3.26}$$

where the spin is represented by up and down arrows. The model includes the spin-flip process in the term with amplitude V, and the non spin-flip process in terms with amplitude t. In the same way as the previous model, the ET transfer process is represented as the linear combination of the nearest neighbor orbitals, with amplitudes being the hopping integrals of the couplings between the orbital in one site and the orbital at the

neighboring atom. Then, since the spin was considered in the ET process, it was necessary to include the spin in the wavefunctions that will be used in the model.

The wavefunctions (Eq. 2.14 and Eq. 2.15) used for the nearest neighbor tight-binding model of Eq. 3.2 and Eq. 3.3 were modified to include spins. The modified wavefunctions are:

$$\Psi_{A\uparrow/\downarrow}(\mathbf{R}_A) = e^{i\mathbf{K}\cdot\mathbf{R}_A}F^{\mathbf{K}}_{A\uparrow/\downarrow}(\mathbf{R}_A) + e^{i\mathbf{K}'\cdot\mathbf{R}_A}F^{\mathbf{K}'}_{A\uparrow/\downarrow}(\mathbf{R}_A),$$

$$\Psi_{B\uparrow/\downarrow}(\mathbf{R}_B) = e^{i\mathbf{K}\cdot\mathbf{R}_B}F^{\mathbf{K}}_{B\uparrow/\downarrow}(\mathbf{R}_B) + e^{i\mathbf{K}'\cdot\mathbf{R}_B}F^{\mathbf{K}'}_{B\uparrow/\downarrow}(\mathbf{R}_B),$$

where the change is in the consideration of spin up or down states. These were simplified as:

$$\Psi_{A\uparrow/\downarrow}(\mathbf{R}_A) = \mathcal{A}^\dagger(\mathbf{R}_A)F_{A\uparrow/\downarrow}(\mathbf{R}_A), \qquad \Psi_{B\uparrow/\downarrow}(\mathbf{R}_B) = \mathcal{B}^\dagger(\mathbf{R}_B)F_{B\uparrow/\downarrow}(\mathbf{R}_B), \tag{3.27}$$

with:

$$F_{I\uparrow/\downarrow}(\mathbf{R}_I) = \begin{pmatrix} F^{\mathbf{K}}_{I\uparrow/\downarrow}(\mathbf{R}_I) \\ F^{\mathbf{K}'}_{I\uparrow/\downarrow}(\mathbf{R}_I) \end{pmatrix},$$

similarly as the simplification done for the previous wavefunctions.

As in the last section, the model for A sites, in Eq. 3.25, was the first being treated. To begin, a substitution was made by defining $\sigma = \uparrow / \downarrow$ and $\sigma' = \downarrow / \uparrow$ to improve the aspect of the equations. Then Eq. 3.27 was substituted, and both sides were multiplied by $\sum_{\mathbf{R}_A} g(\mathbf{r}-\mathbf{R}_A)$, the smoothing function allowing: $F_{I\sigma}(\mathbf{R}) \to F_{I\sigma}(\mathbf{r})$. After, both sides were multiplied by $\mathcal{A}(\mathbf{R}_A)$ to obtain:

$$\begin{aligned}
&\sum_{\mathbf{R}_A} g(\mathbf{r}-\mathbf{R}_A)\varepsilon\mathcal{A}(\mathbf{R}_A)\mathcal{A}^\dagger(\mathbf{R}_A)F_{A\sigma}(\mathbf{r}) = \\
&\sum_{l=1}^{2}\sum_{\mathbf{R}_A} g(\mathbf{r}-\mathbf{R}_A)t^{in}_{\mathbf{R}_{A\sigma},(\mathbf{R}_A+\tau_l^A)_\sigma}\mathcal{A}(\mathbf{R}_A)\mathcal{A}^\dagger(\mathbf{R}_A+\tau_l^A)F_{A\sigma}(\mathbf{r}+\tau_l^A) \\
&+\sum_{l=1}^{2}\sum_{\mathbf{R}_A} g(\mathbf{r}-\mathbf{R}_A)V^{in}_{\mathbf{R}_{A\sigma},(\mathbf{R}_A+\tau_l^A)_{\sigma'}}\mathcal{A}(\mathbf{R}_A)\mathcal{A}^\dagger(\mathbf{R}_A+\tau_l^A)F_{A\sigma'}(\mathbf{r}+\tau_l^A) \\
&+\sum_{\mathbf{R}_A} g(\mathbf{r}-\mathbf{R}_A)t^{out}_{\mathbf{R}_{A\sigma},(\mathbf{R}_A+\tau_3)_\sigma}\mathcal{A}(\mathbf{R}_A)\mathcal{B}^\dagger(\mathbf{R}_A+\tau_3)F_{B\sigma}(\mathbf{r}+\tau_3),
\end{aligned} \tag{3.28}$$

where the products $\mathcal{A}(\mathbf{R}_A)\mathcal{A}^\dagger(\mathbf{R}_A+\tau_\mathbf{l}^\mathbf{A})$ and $\mathcal{A}(\mathbf{R}_A)\mathcal{B}^\dagger(\mathbf{R}_A+\tau_\mathbf{3})$ were previously obtained in Eq. 3.6.

The phonon modulation to the amplitudes was included as previously with Eq. 3.7, and amplitude V was modulated similarly with:

$$V^{in}_{\mathbf{R}_I,\mathbf{R}_I+\tau_l^I} = V^{in}_o - \frac{\eta^{in}V^{in}_o}{c^2}\tau_l^I\cdot[\mathbf{u}_I(\mathbf{R}_I) - \mathbf{u}_{I'}(\mathbf{R}_I+\tau_l^I)],$$

where:

$$\eta^{in} = -\frac{c}{V^{in}_o}\frac{\partial}{\partial c}V^{in}_o,$$

and as discussed, in the model $V^{in}_o = \lambda^{in}_{SO}\nu_l$. Next the Taylor series expansion on the Envelope functions was performed: $F_{I\sigma}(\mathbf{r}+\tau) \approx F_{I\sigma}(\mathbf{r}) + \tau\cdot\nabla F_{I\sigma}(\mathbf{r})$; and again, acoustic and optical phonons were treated separately by using Eq. 3.8. Then Eq. 3.9 and Eq. 3.10

were substituted. Now, given that nothing depends on $\mathbf{R}_A$: $\sum_{\mathbf{R}_A} g(\mathbf{r}-\mathbf{R}_A)=1$. With all these steps, Eq. 3.28 results in:

$$\begin{aligned}\varepsilon F_{A\sigma}(\mathbf{r})\mathbb{1} = &\sum_{l=1}^{2}\left(t_o^{in}+\frac{\beta^{in}t_o^{in}}{c^2}\tau_l^A\cdot[(\tau_l^A\cdot\nabla)(\alpha^{ac}\mathbf{u}(\mathbf{r})+\alpha^{op}\mathbf{v}(\mathbf{r}))]\right)\\ &\begin{pmatrix}e^{i\mathbf{K}\cdot\tau_l^A} & 0\\ 0 & e^{i\mathbf{K}'\cdot\tau_l^A}\end{pmatrix}\left(F_{A\sigma}(\mathbf{r})+\tau_l^A\cdot\nabla F_{A\sigma}(\mathbf{r})\right)\\ &+\sum_{l=1}^{2}\left(\lambda_{SO}^{in}\nu_l+\frac{\eta^{in}\lambda_{SO}^{in}\nu_l}{c^2}\tau_l^A\cdot[(\tau_l^A\cdot\nabla)(\alpha^{ac}\mathbf{u}(\mathbf{r})+\alpha^{op}\mathbf{v}(\mathbf{r}))]\right)\\ &\begin{pmatrix}e^{i\mathbf{K}\cdot\tau_l^A} & 0\\ 0 & e^{i\mathbf{K}'\cdot\tau_l^A}\end{pmatrix}\left(F_{A\sigma'}(\mathbf{r})-\tau_l^A\cdot\nabla F_{A\sigma'}(\mathbf{r})\right)\\ &+\left(t_o^{out}+\frac{\beta^{out}t_o^{out}}{c^2}\tau_3\cdot[(\tau_3\cdot\nabla)(\alpha^{ac}\mathbf{u}(\mathbf{r})-\alpha^{op}\mathbf{v}(\mathbf{r}))-2\alpha^{op}\mathbf{v}(\mathbf{r})]\right)\\ &\begin{pmatrix}e^{i\mathbf{K}\cdot\tau_3} & 0\\ 0 & e^{i\mathbf{K}'\cdot\tau_3}\end{pmatrix}\left(F_{B\sigma}(\mathbf{r})+\tau_3\cdot\nabla F_{B\sigma}(\mathbf{r})\right).\end{aligned}\tag{3.29}$$

By taking terms up to second order in τ_l^A and τ_3 (due to the decay of relevance of high order terms), each term in this equation has three other terms. The first three terms are identical to the previously obtained in Eq. 3.13, Eq. 3.15 and Eq. 3.17 respectively; and the last three correspond to Eq. 3.18, Eq. 3.19 and Eq. 3.21 respectively. The remaining three terms derived from Eq. (3.29) are:

- **4th term.** This term is the first order intrinsic SO overlap. The derivation was as follows:

$$\sum_{l=1}^{2}\lambda_{SO}^{in}\nu_l\begin{pmatrix}e^{i\mathbf{K}\cdot\tau_l^A} & 0\\ 0 & e^{i\mathbf{K}'\cdot\tau_l^A}\end{pmatrix}F_{A\sigma'}(\mathbf{r})=\sum_{l=1}^{2}\lambda_{SO}^{in}\begin{pmatrix}e^{i\mathbf{K}\cdot\tau_l^A}\nu_l & 0\\ 0 & e^{i\mathbf{K}'\cdot\tau_l^A}\nu_l\end{pmatrix}F_{A\sigma'}(\mathbf{r}),$$

  where the sums resulted in:

$$\sum_{l=1}^{2}e^{i\mathbf{K}\cdot\tau_l^A}\nu_l=e^{i\frac{\pi}{2}}-e^{-i\frac{\pi}{2}}=2i\sin(\frac{\pi}{2})=2i,\quad \sum_{l=1}^{2}e^{i\mathbf{K}'\cdot\tau_l^A}\nu_l=-2i,$$

  so the term ended up as:

$$\lambda_{SO}^{in}\begin{pmatrix}2i & 0\\ 0 & -2i\end{pmatrix}F_{A\sigma'}(\mathbf{r})=2i\nu\lambda_{SO}^{in}F_{A\sigma'}(\mathbf{r}).$$

  This indicates that the first order intra-helix ET occurs as a spin-flip process instead of a non spin-flip process as the latter vanishes at first order. The reason for this term not disappearing relies on the term ν_l that appears due to the intrinsic SO coupling. Also, this term changes sign with $\mathbf{K}$ as in the intra-helix of the previous model.

- **5th term.** This term is the second order contribution of the previous one. The calculation was:

$$\sum_{l=1}^{2}\lambda_{SO}^{in}\nu_l\begin{pmatrix}e^{i\mathbf{K}\cdot\tau_l^A} & 0\\ 0 & e^{i\mathbf{K}'\cdot\tau_l^A}\end{pmatrix}\tau_l^A\cdot\nabla F_{A\sigma'}(\mathbf{r})$$
$$=\sum_{l=1}^{2}\lambda_{SO}^{in}\begin{pmatrix}e^{i\mathbf{K}\cdot\tau_l^A}\nu_l\tau_l^A & 0\\ 0 & e^{i\mathbf{K}'\cdot\tau_l^A}\nu_l\tau_l^A\end{pmatrix}\cdot\nabla F_{A\sigma'}(\mathbf{r}),$$

where the sums were:

$$\sum_{l=1}^{2}e^{i\mathbf{K}\cdot\tau_l^A}\nu_l\tau_l^A=e^{i\frac{\pi}{2}}(a\Delta\phi\hat{\mathrm{y}}+\frac{b\Delta\phi}{2\pi}\hat{\mathrm{z}})+e^{-i\frac{\pi}{2}}(a\Delta\phi\hat{\mathrm{y}}+\frac{b\Delta\phi}{2\pi}\hat{\mathrm{z}})$$
$$=2(a\Delta\phi\hat{\mathrm{y}}+\frac{b\Delta\phi}{2\pi}\hat{\mathrm{z}})(\cos(\frac{\pi}{2}))=0,$$
$$\sum_{l=1}^{2}e^{i\mathbf{K}'\cdot\tau_l^A}\nu_l\tau_l^A=0,$$

so it was obtained:

$$\lambda_{SO}^{in}\begin{pmatrix}0 & 0\\ 0 & 0\end{pmatrix}F_{A\sigma'}(\mathbf{r})=0.$$

This means that there is no second order contribution of the intra-helix spin-flip ET. The cause is again the same as why the first order term didn't vanish. Then in the intra-helix there is either first or second order but not both contributions. Then the intrinsic SO appears only as a first order contribution in the intra-helix.

- **6th term.** Finally, this term is the spin-phonon in the intra-helix with spin-flip overlap. This term includes the phonon effect, and the intrinsic SO effect. The calculation was made as:

$$\sum_{l=1}^{2}\frac{\eta^{in}\lambda_{SO}^{in}\nu_l}{c^2}\tau_l^A\cdot[(\tau_l^A\cdot\nabla)(\alpha^{ac}\mathbf{u}(\mathbf{r})+\alpha^{op}\mathbf{v}(\mathbf{r}))]\begin{pmatrix}e^{i\mathbf{K}\cdot\tau_l^A} & 0\\ 0 & e^{i\mathbf{K}'\cdot\tau_l^A}\end{pmatrix}F_{A\sigma'}(\mathbf{r})$$
$$=\frac{\eta^{in}\lambda_{SO}^{in}}{c^2}\begin{pmatrix}\sum_{l=1}^{2}e^{i\mathbf{K}\cdot\tau_l^A}\nu_l\tau_l^A(\tau_l^A\cdot\nabla) & 0\\ 0 & \sum_{l=1}^{2}e^{i\mathbf{K}'\cdot\tau_l^A}\nu_l\tau_l^A(\tau_l^A\cdot\nabla)\end{pmatrix}$$
$$\cdot(\alpha^{ac}\mathbf{u}(\mathbf{r})+\alpha^{op}\mathbf{v}(\mathbf{r}))F_{A\sigma'}(\mathbf{r}),$$

where the sums were:

$$\sum_{l=1}^{2}e^{i\mathbf{K}\cdot\tau_l^A}\nu_l\tau_l^A(\tau_l^A\cdot\nabla)$$
$$=e^{i\frac{\pi}{2}}(a\Delta\phi\hat{\mathrm{y}}+\frac{b\Delta\phi}{2\pi}\hat{\mathrm{z}})(a\Delta\phi\partial_y+\frac{b\Delta\phi}{2\pi}\partial_z)-e^{-i\frac{\pi}{2}}(-a\Delta\phi\hat{\mathrm{y}}-\frac{b\Delta\phi}{2\pi}\hat{\mathrm{z}})(-a\Delta\phi\partial_y-\frac{b\Delta\phi}{2\pi}\partial_z)$$
$$=2i(a\Delta\phi\hat{\mathrm{y}}+\frac{b\Delta\phi}{2\pi}\hat{\mathrm{z}})(a\Delta\phi\partial_y+\frac{b\Delta\phi}{2\pi}\partial_z)\sin(\frac{\pi}{2})=2i(a\Delta\phi\hat{\mathrm{y}}+\frac{b\Delta\phi}{2\pi}\hat{\mathrm{z}})(a\Delta\phi\partial_y+\frac{b\Delta\phi}{2\pi}\partial_z),$$
$$\sum_{l=1}^{2}e^{i\mathbf{K}'\cdot\tau_l^A}\nu_l\tau_l^A(\tau_l^A\cdot\nabla)=-2i(a\Delta\phi\hat{\mathrm{y}}+\frac{b\Delta\phi}{2\pi}\hat{\mathrm{z}})(a\Delta\phi\partial_y+\frac{b\Delta\phi}{2\pi}\partial_z);$$

so the term resulted in:

$$\frac{\eta^{in}\lambda_{SO}^{in}}{c^2}\begin{pmatrix} 2i(a\Delta\phi\hat{\mathrm{y}}+\frac{b\Delta\phi}{2\pi}\hat{\mathrm{z}})(a\Delta\phi\partial_y+\frac{b\Delta\phi}{2\pi}\partial_z) & 0 \\ 0 & -2i(a\Delta\phi\hat{\mathrm{y}}+\frac{b\Delta\phi}{2\pi}\hat{\mathrm{z}})(a\Delta\phi\partial_y+\frac{b\Delta\phi}{2\pi}\partial_z)\end{pmatrix}$$
$$\cdot[(\tau_l^A\cdot\nabla)(\alpha^{ac}\mathbf{u}(\mathbf{r})+\alpha^{op}\mathbf{v}(\mathbf{r}))]F_{A\sigma'}(\mathbf{r})=$$
$$\nu\frac{\eta^{in}\lambda_{SO}^{in}}{c^2}2i(a\Delta\phi\hat{\mathrm{y}}+\frac{b\Delta\phi}{2\pi}\hat{\mathrm{z}})(a\Delta\phi\partial_y+\frac{b\Delta\phi}{2\pi}\partial_z)\cdot(\tau_l^A\cdot\nabla)(\alpha^{ac}\mathbf{u}(\mathbf{r})+\alpha^{op}\mathbf{v}(\mathbf{r}))\nu F_{A\sigma'}(\mathbf{r}).$$

The following product that resulted from the procedure was calculated as:

$$(a\Delta\phi\hat{\mathrm{y}}+\frac{b\Delta\phi}{2\pi}\hat{\mathrm{z}})(a\Delta\phi\partial_y+\frac{b\Delta\phi}{2\pi}\partial_z)(\alpha^{ac}\mathbf{u}(\mathbf{r})+\alpha^{op}\mathbf{v}(\mathbf{r}))=$$
$$(a\Delta\phi\hat{\mathrm{y}}+\frac{b\Delta\phi}{2\pi}\hat{\mathrm{z}})\cdot(a\Delta\phi\alpha^{ac}(\partial_y u_x\hat{\mathrm{x}}+\partial_y u_y\hat{\mathrm{y}}+\partial_y u_z\hat{\mathrm{z}})+a\Delta\phi\alpha^{op}(\partial_y v_x\hat{\mathrm{x}}+\partial_y v_y\hat{\mathrm{y}}+\partial_y v_z\hat{\mathrm{z}})$$
$$+\frac{b\Delta\phi}{2\pi}\alpha^{ac}(\partial_z u_x\hat{\mathrm{x}}+\partial_z u_y\hat{\mathrm{y}}+\partial_z u_z\hat{\mathrm{z}})+\frac{b\Delta\phi}{2\pi}\alpha^{op}(\partial_z v_x\hat{\mathrm{x}}+\partial_z v_y\hat{\mathrm{y}}+\partial_z v_z\hat{\mathrm{z}}))=$$
$$a^2\Delta\phi^2(\alpha^{ac}\partial_y u_y+\alpha^{op}\partial_y v_y)+\frac{ab\Delta\phi^2}{2\pi}(\alpha^{ac}(\partial_z u_y+\partial_y u_z)+\alpha^{op}(\partial_y v_z+\partial_z v_y))$$
$$+\frac{b^2\Delta\phi^2}{4\pi^2}(\alpha^{ac}\partial_z u_z+\alpha^{op}\partial_z v_z),$$

so the final result was:

$$\sum_{l=1}^{2}\frac{\eta^{in}\lambda_{SO}^{in}\nu_l}{c^2}\tau_l^A\cdot[(\tau_l^A\cdot\nabla)(\alpha^{ac}\mathbf{u}(\mathbf{r})+\alpha^{op}\mathbf{v}(\mathbf{r}))]\begin{pmatrix}e^{i\mathbf{K}\cdot\tau_l^A} & 0\\ 0 & e^{i\mathbf{K}'\cdot\tau_l^A}\end{pmatrix}F_{A\sigma'}(\mathbf{r})$$
$$=\nu\frac{\eta^{in}\lambda_{SO}^{in}}{c^2}2i[a^2\Delta\phi^2(\alpha^{ac}\partial_y u_y+\alpha^{op}\partial_y v_y)+\frac{ab\Delta\phi^2}{2\pi}(\alpha^{ac}(\partial_z u_y+\partial_y u_z)$$
$$+\alpha^{op}(\partial_y v_z+\partial_z v_y))+\frac{b^2\Delta\phi^2}{4\pi^2}(\alpha^{ac}\partial_z u_z+\alpha^{op}\partial_z v_z)]\nu F_{A\sigma'}(\mathbf{r}).$$

The result indicates that spin-phonon interaction mediates the inter-helix spin-flip ET and that the optical and acoustical amplitudes have equal relevance in this process. An important observation is that phonon amplitude in $\hat{y}$ has a different coefficient than in $\hat{z}$, and that the amplitude in $\hat{x}$ does not affect the process. This means that the vibration modes will have different effects on the ET, and that there is a mode with maximum and one with minimum perturbation in the process.

By adding all the nine terms it was obtained:

$$\varepsilon F_{A\sigma}(\mathbf{r})\mathbb{1}=-t^{in}2R\nu k_y F_{A\sigma}(\mathbf{r})+\left(1+\frac{\eta^{in}\Delta\phi^2}{c^2}[a^2(\alpha^{ac}\partial_y u_y+\alpha^{op}\partial_y v_y)+\frac{ab}{2\pi}(\alpha^{ac}\right.$$
$$\left.\times(\partial_z u_y+\partial_y u_z)+\alpha^{op}(\partial_y v_z+\partial_z v_y))+\frac{b^2}{4\pi^2}(\alpha^{ac}\partial_z v_z+\alpha^{op}\partial_z v_z)]\right)2i\nu\lambda_{SO}^{in}F_{A\sigma'}(\mathbf{r})$$
$$+\left(1-2aik_x+\frac{4\beta^{out}}{c^2}(a^2\partial_x(\alpha^{ac}u_x-\alpha^{op}v_x)+a\alpha^{op}v_x)\right)t_o^{out}\mathbb{1}F_{B\sigma}(\mathbf{r}).$$

This shows that the results for the non spin-flip ET process are the same that for the electron-phonon model, but the implementation of spin added the intra-helix spin-flip term which contains the first order intrinsic SO effect and the spin-phonon effects.

By following a similar procedure for the equation for B sites, Eq. 3.26, it resulted in:

$$\varepsilon F_{B\sigma}(\mathbf{r})\mathbb{1} = -t^{in}2R\nu k_y F_{B\sigma}(\mathbf{r}) + \left(1 + \frac{\eta^{in}\Delta\phi^2}{c^2}[a^2(\alpha^{ac}\partial_y u_y - \alpha^{op}\partial_y v_y) + \frac{ab}{2\pi}(\alpha^{ac} \times (\partial_z u_y + \partial_y u_z) - \alpha^{op}(\partial_y v_z + \partial_z v_y)) + \frac{b^2}{4\pi^2}(\alpha^{ac}\partial_z v_z - \alpha^{op}\partial_z v_z)]\right) 2i\nu\lambda_{SO}^{in} F_{B\sigma'}(\mathbf{r}) + \left(1 + 2aik_x + \frac{4\beta^{out}}{c^2}(a^2\partial_x(\alpha^{ac}u_x - \alpha^{op}v_x) + a\alpha^{op}v_x)\right) t_o^{out}\mathbb{1}F_{A\sigma}(\mathbf{r}).$$

Here the non spin-flip terms change in the same way as before for the electron-phonon model. For the spin-flip process, the spin-phonon term changes sign together with the optical amplitudes so in overall, the acoustical amplitudes are the ones that change sign. The overall meaning of the equation is the same as the one for A sites.

By substituting some of the long terms from the equations of A and B sites:

$$\gamma^{in} = \left(1 + \frac{\eta^{in}}{c^2}[a^2\Delta\phi^2(\alpha^{ac}\partial_y u_y + \alpha^{op}\partial_y v_y) + \frac{ab\Delta\phi^2}{2\pi}(\alpha^{ac}(\partial_z u_y + \partial_y u_z) + \alpha^{op}(\partial_y v_z + \partial_z v_y)) + \frac{b^2\Delta\phi^2}{4\pi^2}(\alpha^{ac}\partial_z v_z + \alpha^{op}\partial_z v_z)]\right),$$

$$\gamma^{out} = \left(1 - 2aik_x + \frac{4\beta^{out}}{c^2}(a^2\partial_x(\alpha^{ac}u_x - \alpha^{op}v_x) + a\alpha^{op}v_x)\right),$$

the full Schrödinger equation is written as in Eq.3.22 with the definitions in Eq. 3.23, where: $\mathbf{F}^{\mathbf{K}^{(\prime)}}(\mathbf{r}) = (\mathbf{F}^{\mathbf{K}^{(\prime)}}_{A\uparrow}(\mathbf{r}), \mathbf{F}^{\mathbf{K}^{(\prime)}}_{A\downarrow}(\mathbf{r}), \mathbf{F}^{\mathbf{K}^{(\prime)}}_{B\uparrow}(\mathbf{r}), \mathbf{F}^{\mathbf{K}^{(\prime)}}_{B\downarrow}(\mathbf{r}))$, and:

$$\mathcal{H}^{\mathbf{K},\mathbf{K}'} = \begin{pmatrix} -2Rt_o^{in}k_y\nu & 2i\gamma^{in}\lambda_{SO}^{in}\nu & \gamma^{out}t_o^{out} & 0 \\ -2i\gamma^{in}\lambda_{SO}^{in}\nu & -2Rt_o^{in}k_y\nu & 0 & \gamma^{out}t_o^{out} \\ \gamma^{out\dagger}t_o^{out} & 0 & -2Rt_o^{in}k_y\nu & 2i\gamma^{in}\lambda_{SO}^{in}\nu \\ 0 & \gamma^{out\dagger}t_o^{out} & -2i\gamma^{in}\lambda_{SO}^{in}\nu & -2Rt_o^{in}k_y\nu \end{pmatrix}. \tag{3.30}$$

The estimated values in addition to the previous ones, were obtained from Varela[81]: $\lambda_{SO}^{in} = 0.671$ meV.

The diagonal terms, $-2Rt_o^{in}k_y\nu$, are the kinetic terms that couple the intra-helix non spin-flip ET, which have the same value as the electron-phonon model. The inter-helix term with no spin-flip is $\gamma_A^{out\dagger}t_o^{out\dagger}$ for $A \to B$ and $\gamma_B^{out\dagger}t_o^{out\dagger}$ for $B \to A$, where each has three terms containing both first and second order kinetic terms and electron-phonon contribution. By comparison with the previous results in Eq. 3.24, it can be observed that the new results in Eq. 3.30 contain the previous ones, thus the new results are additive and the consequences should be too.

Now the results from Varela et al. in Eq. 2.10 are compared. Their intra-helix intrinsic SO term with spin-flip is: $-2\nu\lambda_{SO}^{in}\mathbf{1}_{\sigma'}s_y$, and the ones obtained are: $2i\gamma_{A,B}^{in}\lambda_{SO}^{in}\nu$ for A, B sites. It can be seen that there is a miss-match between the terms that could be solved by multiplying by is_y on the last result. This missing factor originates from the coupled equations in Eq. 2.9, and it will need to be addressed in future a work continuing this methodology.

Regardless of this miss-match that could be solved, some consequences may be taken in account. In the result obtained in this work, there are two terms in the intra-helix spin-flip: the first order intrinsic SO term and the spin-phonon contribution. The inter-helix term with spin-flip is 0, which is due to the fact that the Rashba effect is not considered since no electric field is present in the model.

Spin-phonon interaction affects the intra-helix ET with spin-flip process, where the optical and acoustical amplitudes are both second order, but in the B site regime the acoustical amplitude changes sign. There is also a first order kinetic contribution.

The non spin-flip ET has twice more terms than in the spin-flip process, which is mediated by the first order kinetic and spin-phonon interactions. Then one would expect that the process with less parameters, spin-flip, will be more manipulable. Nevertheless, phonon amplitudes are the ones that can be controlled in the model thus only the spin-flip process and the inter-helix ET can be tuned with the phonon bath.

The most important conclusion is the fact that optical amplitudes appear at first order while acoustical amplitudes appear at second order. Then in a set up where optical phonons can be controlled while acoustical are suppressed or viceversa, the inter-helix ET will show different behavior.

Chapter 4

Conclusions and future work

The structure used for the DNA model was presented and the considerations were: a B-form DNA with a uniform base sequence, 10 nucleotides per turn of the helix, spinless electrons for the first model, π orbitals, and no source of electrical field. Then the models for electron-phonon and spin-phonon interaction were developed. The main results include that the intra-helix non spin-flip ET only includes a second order kinetic term, while the electron-phonon interaction is present between helices and the spin-phonon interaction appears for intra-helix spin-flip ET. The parameters in the model were obtained from the literature.

There were no differences between models as the second one contained the terms in the first and added the extra terms due to the intrinsic SO interaction. Therefore, the addition of this effect did not change the results from the previous (e-phonon) model. While the electron-phonon interaction is able to predict that phonons are relevant only in inter-helix ET and that optical modes have much more impact, the spin-phonon interaction adds that intrinsic SO affects the spin-flip processes in intra-helix ET.

In comparison with the results from Varela et al.[81], the electron-phonon model replicated their results while in the spin-phonon model the results had a miss-match. This miss-match could be solved in a future work to support the observed consequences.

This model was able to describe the interactions proposed for ET in DNA that are present at physiological conditions, and explain the large coherence lengths observed experimentally due to a partial protection coming from the fact that acoustical phonons only have a second order contribution. This will affect the development of spintronic devices as the mechanism underlying their development could be described using a similar model.

While the model can qualitatively describe the effect of phonons and spin in ET, a quantitative description remains to be done. Nevertheless, quantitative analyses are not necessary to expose the behavior of interactions such as phonon or spin, which can be properly analyzed on a qualitative approach.

This model can be modified to include other interactions such as polarons or the effect of electric fields in a similar way by perturbations. However, it is always necessary to consider if the new addition affects other contributions more than enough to change the approach.

In the future, it will be interesting to use this model to describe ET of other organic or inorganic molecules such as oligopeptides, in a general structure similar to the work of Torres et al.[90], or others in the spotlight of molecular spintronics. Also, trying to add other interactions or improve the model could reveal opportunities to predict important consequences for the use of DNA and similar molecules in the future of spintronic devices.

Bibliography

[1] Jane Grimwood, Laurie A Gordon, Anne Olsen, Astrid Terry, Jeremy Schmutz, Jane Lamerdin, Uffe Hellsten, David Goodstein, Olivier Couronne, Mary Tran-Gyamfi, et al. The dna sequence and biology of human chromosome 19. Nature, 428(6982):529–535, 2004.

[2] Jonathan D Vaught, Chris Bock, Jeff Carter, Tim Fitzwater, Matt Otis, Dan Schneider, Justin Rolando, Sheela Waugh, Sheri K Wilcox, and Bruce E Eaton. Expanding the chemistry of dna for in vitro selection. Journal of the American Chemical Society, 132(12):4141–4151, 2010.

[3] Francis Collins. The language of life: DNA and the revolution in personalised medicine. Profile Books, 2010.

[4] Gianaurelio Cuniberti, E Maciá, A Rodriguez, and RA Römer. Tight-binding modeling of charge migration in dna devices. In Charge Migration in DNA, pages 1–20. Springer, 2007.

[5] Shana O Kelley and Jacqueline K Barton. Electron transfer between bases in double helical dna. Science, 283(5400):375–381, 1999.

[6] Gianaurelio Cuniberti, Luis Craco, Danny Porath, and Cees Dekker. Backbone-induced semiconducting behavior in short dna wires. Physical review b, 65(24):241314, 2002.

[7] Yuan-Jie Ye and Yan Jiang. Electronic structures and long-range electron transfer through dna molecules. International Journal of Quantum Chemistry, 78(2):112–130, 2000.

[8] Jinyi Dong, Chao Zhou, and Qiangbin Wang. Towards active self-assembly through dna nanotechnology. DNA Nanotechnology, pages 1–25, 2020.

[9] Jie Chen, Ying Zhu, Huajie Liu, and Lihua Wang. Tailoring dna self-assembly to build hydrogels. DNA Nanotechnology, pages 27–56, 2020.

[10] Xuemei Xu, Pia Winterwerber, David Ng, and Yuzhou Wu. Dna-programmed chemical synthesis of polymers and inorganic nanomaterials. DNA Nanotechnology, pages 57–81, 2020.

[11] Chunhai Fan and Yonggang Ke. DNA Nanotechnology: From Structure to Functionality. Springer Nature, 2020.

[12] Nadrian C Seeman and Hanadi F Sleiman. Dna nanotechnology. Nature Reviews Materials, 3(1):1–23, 2017.

[13] Anirban Ghosh and Manju Bansal. A glossary of dna structures from a to z. Acta Crystallographica Section D: Biological Crystallography, 59(4):620–626, 2003.

[14] Robert Cecil Olby. The path to the double helix: the discovery of DNA. Courier Corporation, 1994.

[15] Richard R Sinden. DNA structure and function. Gulf Professional Publishing, 1994.

[16] Jeremy M Berg, John L Tymoczko, and Lubert Stryer. Biochemistry, ; w. h. New York: Freeman and Company: New York, 2002.

[17] Lawrence Hunter. Molecular biology for computer scientists. Artificial intelligence and molecular biology, 177:1–46, 1993.

[18] Shahana Yasmin Chowdhury, Swakkhar Shatabda, and Abdollah Dehzangi. idnaprotes: Identification of dna-binding proteins using evolutionary and structural features. Scientific reports, 7(1):1–14, 2017.

[19] Massimiliano Di Ventra and Yuriy V Pershin. Dna spintronics sees the light. Nature nanotechnology, 6(4):198–199, 2011.

[20] JF Gregg, I Petej, E Jouguelet, and C Dennis. Spin electronics—a review. Journal of Physics D: Applied Physics, 35(18):R121, 2002.

[21] SA Wolf, DD Awschalom, RA Buhrman, JM Daughton, von S von Molnár, ML Roukes, A Yu Chtchelkanova, and DM Treger. Spintronics: a spin-based electronics vision for the future. science, 294(5546):1488–1495, 2001.

[22] SD Bader and SSP Parkin. Spintronics. Annu. Rev. Condens. Matter Phys., 1(1):71–88, 2010.

[23] Stefano Sanvito. Molecular spintronics. Chemical Society Reviews, 40(6):3336–3355, 2011.

[24] Alexandre R Rocha, Victor M Garcia-Suarez, Steve W Bailey, Colin J Lambert, Jaime Ferrer, and Stefano Sanvito. Towards molecular spintronics. Nature materials, 4(4):335–339, 2005.

[25] Masashi Shiraishi and Tadaaki Ikoma. Molecular spintronics. Physica E: Low-dimensional Systems and Nanostructures, 43(7):1295–1317, 2011.

[26] Lapo Bogani and Wolfgang Wernsdorfer. Molecular spintronics using single-molecule magnets. In Nanoscience and technology: a collection of reviews from nature journals, pages 194–201. World Scientific, 2010.

[27] David Winogradoff, Pin-Yi Li, Himanshu Joshi, Lauren Quednau, Christopher Maffeo, and Aleksei Aksimentiev. Chiral systems made from dna. Advanced Science, 8(5):2003113, 2021.

[28] Ching Tsang, Robert E Fontana, Tsann Lin, David E Heim, Virgil S Speriosu, Bruce A Gurney, and Mason L Williams. Design, fabrication and testing of spin-valve read heads for high density recording. IEEE Transactions on Magnetics, 30(6):3801–3806, 1994.

[29] M Zwolak and M Di Ventra. Dna spintronics. Applied Physics Letters, 81(5):925–927, 2002.

[30] Geert LJA Rikken. A new twist on spintronics. science, 331(6019):864–865, 2011.

[31] Ron Naaman and David H Waldeck. Chiral-induced spin selectivity effect. The journal of physical chemistry letters, 3(16):2178–2187, 2012.

[32] B Göhler, V Hamelbeck, TZ Markus, M Kettner, GF Hanne, Z Vager, R Naaman, and H Zacharias. Spin selectivity in electron transmission through self-assembled monolayers of double-stranded dna. Science, 331(6019):894–897, 2011.

[33] Zouti Xie, Tal Z Markus, Sidney R Cohen, Zeev Vager, Rafael Gutierrez, and Ron Naaman. Spin specific electron conduction through dna oligomers. Nano letters, 11(11):4652–4655, 2011.

[34] Sina Yeganeh, Mark A Ratner, Ernesto Medina, and Vladimiro Mujica. Chiral electron transport: Scattering through helical potentials. The Journal of chemical physics, 131(1):014707, 2009.

[35] See-Hun Yang, Ron Naaman, Yossi Paltiel, and Stuart SP Parkin. Chiral spintronics. Nature Reviews Physics, 3(5):328–343, 2021.

[36] S Behnia, S Fathizadeh, and A Akhshani. Dna spintronics: Charge and spin dynamics in dna wires. The Journal of Physical Chemistry C, 120(5):2973–2983, 2016.

[37] E Diaz, RPA Lima, and F Dominguez-Adame. Bloch-like oscillations in the peyrard-bishop-holstein model. Physical Review B, 78(13):134303, 2008.

[38] GS Diniz, A Latgé, and SE Ulloa. Helicoidal fields and spin polarized currents in carbon nanotube–dna hybrids. Physical review letters, 108(12):126601, 2012.

[39] Md Wazedur Rahman, Kazi M Alam, and Sandipan Pramanik. Long carbon nanotubes functionalized with dna and implications for spintronics. ACS omega, 3(12):17108–17115, 2018.

[40] Michael D Purugganan, Challa V Kumar, Nicholas J Turro, and Jacqueline K Barton. Accelerated electron transfer between metal complexes mediated by dna. Science, 241(4873):1645–1649, 1988.

[41] Fabien Boussicault and Marc Robert. Electron transfer in dna and in dna-related biological processes. electrochemical insights. Chemical Reviews, 108(7):2622–2645, 2008.

[42] Hans-Achim Wagenknecht. Electron transfer processes in dna: mechanisms, biological relevance and applications in dna analytics. Natural Product Reports, 23(6):973–1006, 2006.

[43] M Bixon, Bernd Giese, Stephan Wessely, Thomas Langenbacher, Maria E Michel-Beyerle, and Joshua Jortner. Long-range charge hopping in dna. Proceedings of the National Academy of Sciences, 96(21):11713–11716, 1999.

[44] Michael J Heller. Dna microarray technology: devices, systems, and applications. Annual review of biomedical engineering, 4(1):129–153, 2002.

[45] Dayong Yang, Michael J Campolongo, Thua Nguyen Nhi Tran, Roanna CH Ruiz, Jason S Kahn, and Dan Luo. Novel dna materials and their applications. Wiley Interdisciplinary Reviews: Nanomedicine and Nanobiotechnology, 2(6):648–669, 2010.

[46] Bernd Giese, Stephan Wessely, Martin Spormann, Ute Lindemann, Eric Meggers, and Maria E Michel-Beyerle. On the mechanism of long-range electron transfer through dna. Angewandte Chemie International Edition, 38(7):996–998, 1999.

[47] Bernd Giese. Electron transfer in dna. Current opinion in chemical biology, 6(5):612–618, 2002.

[48] Daniel B Hall, R Erik Holmlin, and Jacqueline K Barton. Oxidative dna damage through long-range electron transfer. Nature, 382(6593):731–735, 1996.

[49] Dalibor Chevizovich, Davide Michieletto, Alain Mvogo, Farit Zakiryanov, and Slobodan Zdravković. A review on nonlinear dna physics. Royal Society open science, 7(11):200774, 2020.

[50] EB Starikov*. Electron–phonon coupling in dna: a systematic study. Philosophical Magazine, 85(29):3435–3462, 2005.

[51] Isao Saito, Masami Takayama, Hiroshi Sugiyama, Kazuhiko Nakatani, Akira Tsuchida, and Masahide Yamamoto. Photoinduced dna cleavage via electron transfer: demonstration that guanine residues located 5'to guanine are the most electron-donating sites. Journal of the american chemical society, 117(23):6406–6407, 1995.

[52] Martín Félix and Alexander A Voityuk. Parameters for excess electron transfer in dna. estimation using unoccupied kohn- sham orbitals and td dft. The Journal of Physical Chemistry A, 112(38):9043–9049, 2008.

[53] Yukun Bian and Nanrong Zhao. Dynamic disorder in dna unzipping from single molecule pulling experiments: an analysis based on generalized langevin equation. SCIENTIA SINICA Chimica, 45(4):419–426, 2015.

[54] Sairam S Mallajosyula and Swapan K Pati. Toward dna conductivity: a theoretical perspective. The Journal of Physical Chemistry Letters, 1(12):1881–1894, 2010.

[55] Khatcharin Siriwong and Alexander A Voityuk. π stack structure and hole transfer couplings in dna hairpins and dna. a combined qm/md study. The Journal of Physical Chemistry B, 112(27):8181–8187, 2008.

[56] Daniel Kurnia Suhendro, Efta Yudiarsah, and Rosari Saleh. Effect of phonons and backbone disorder on electronic transport in dna. Physica B: Condensed Matter, 405(23):4806–4811, 2010.

[57] Hirotaka Sugawara. Quantum theory of dnaan approach to electron transfer in dna. Progress of Theoretical Physics Supplement, 164:17–27, 2006.

[58] Mario González-Jiménez, Gopakumar Ramakrishnan, Thomas Harwood, Adrian J Lapthorn, Sharon M Kelly, Elizabeth M Ellis, and Klaas Wynne. Observation of coherent delocalized phonon-like modes in dna under physiological conditions. Nature communications, 7(1):1–6, 2016.

[59] Ludmil B Alexandrov, Kim Ø Rasmussen, Alan R Bishop, and Boian S Alexandrov. Evaluating the role of coherent delocalized phonon-like modes in dna cyclization. Scientific reports, 7(1):1–8, 2017.

[60] Ryan M Harrison, Flavio Romano, Thomas E Ouldridge, Ard A Louis, and Jonathan PK Doye. Identifying physical causes of apparent enhanced cyclization of short dna molecules with a coarse-grained model. Journal of chemical theory and computation, 15(8):4660–4672, 2019.

[61] S Zeković, Slobodan Zdravković, and Zoran Ivić. Charge transfer in dna: the role of large polarons. In Journal of Physics: Conference Series, volume 329, page 012015. IOP Publishing, 2011.

[62] Mayra Peralta, Steven Feijoo, Solmar Varela, Vladimiro Mujica, and Ernesto Medina. Coherence preservation and electron–phonon interaction in electron transfer in dna. The Journal of Chemical Physics, 153(16):165102, 2020.

[63] Esther M Conwell and Svetlana V Rakhmanova. Polarons in dna. Proceedings of the National Academy of Sciences, 97(9):4556–4560, 2000.

[64] Peng-Bo Li, Yuan Zhou, Wei-Bo Gao, and Franco Nori. Enhancing spin-phonon and spin-spin interactions using linear resources in a hybrid quantum system. Physical Review Letters, 125(15):153602, 2020.

[65] Alessandro Lunghi and Stefano Sanvito. How do phonons relax molecular spins? Science advances, 5(9):eaax7163, 2019.

[66] Marc Ganzhorn, Svetlana Klyatskaya, Mario Ruben, and Wolfgang Wernsdorfer. Strong spin–phonon coupling between a single-molecule magnet and a carbon nanotube nanoelectromechanical system. Nature nanotechnology, 8(3):165–169, 2013.

[67] Alessandro Lunghi, Federico Totti, Stefano Sanvito, and Roberta Sessoli. Intramolecular origin of the spin-phonon coupling in slow-relaxing molecular magnets. Chemical science, 8(9):6051–6059, 2017.

[68] A Milosavljević, A Šolajić, J Pešić, Yu Liu, Cedomir Petrovic, N Lazarević, ZV Popović, et al. Evidence of spin-phonon coupling in crsite 3. Physical Review B, 98(10):104306, 2018.

[69] WS Ferreira, J Agostinho Moreira, A Almeida, MR Chaves, JP Araújo, JB Oliveira, JM Machado Da Silva, MA Sá, TM Mendonça, P Simeão Carvalho, et al. Spin-phonon coupling and magnetoelectric properties: Eumno 3 versus gdmno 3. Physical Review B, 79(5):054303, 2009.

[70] Lifa Zhang and Qian Niu. Angular momentum of phonons and the einstein–de haas effect. Physical Review Letters, 112(8):085503, 2014.

[71] DA Garanin and EM Chudnovsky. Angular momentum in spin-phonon processes. Physical Review B, 92(2):024421, 2015.

[72] Samuel J Whiteley, Gary Wolfowicz, Christopher P Anderson, Alexandre Bourassa, He Ma, Meng Ye, Gerwin Koolstra, Kevin J Satzinger, Martin V Holt, F Joseph Heremans, et al. Spin–phonon interactions in silicon carbide addressed by gaussian acoustics. Nature Physics, 15(5):490–495, 2019.

[73] DJ Lockwood and MG Cottam. The spin-phonon interaction in fef2 and mnf2 studied by raman spectroscopy. Journal of Applied Physics, 64(10):5876–5878, 1988.

[74] H Grimm and A Rupprecht. Inelastic neutron scattering studies of oriented dna. In Nonlinear excitations in biomolecules, pages 101–115. Springer, 1995.

[75] H Grimm and A Rupprecht. Low frequency dynamics of dna. Physica B: Condensed Matter, 234:183–187, 1997.

[76] Kohta Ishikawa and Tsuneya Ando. Optical phonon interacting with electrons in carbon nanotubes. Journal of the Physical Society of Japan, 75(8):084713–084713, 2006.

[77] Hidekatsu Suzuura and Tsuneya Ando. Phonons and electron-phonon scattering in carbon nanotubes. Physical review B, 65(23):235412, 2002.

[78] John C Slater and George F Koster. Simplified lcao method for the periodic potential problem. Physical Review, 94(6):1498, 1954.

[79] Charles Kittel, Paul McEuen, and Paul McEuen. Introduction to solid state physics, volume 8. Wiley New York, 1996.

[80] Hassan Raza. Graphene nanoelectronics: metrology, synthesis, properties and applications. Springer Science & Business Media, 2012.

[81] Solmar Varela, Vladimiro Mujica, and Ernesto Medina. Effective spin-orbit couplings in an analytical tight-binding model of dna: Spin filtering and chiral spin transport. Physical Review B, 93(15):155436, 2016.

[82] Edward Uhler Condon, EU Condon, and GH Shortley. The theory of atomic spectra. Cambridge University Press, 1935.

[83] Brian Harold Bransden and Charles Jean Joachain. Physics of atoms and molecules. Pearson Education India, 2003.

[84] Sverre Froyen and Walter A Harrison. Elementary prediction of linear combination of atomic orbitals matrix elements. Physical Review B, 20(6):2420, 1979.

[85] Walter A Harrison. The physics of solid state chemistry. In Festkörperprobleme 17, pages 135–155. Springer, 1977.

[86] Tsuneya Ando. Spin-orbit interaction in carbon nanotubes. Journal of the Physical Society of Japan, 69(6):1757–1763, 2000.

[87] Christian Schüller. Inelastic light scattering of semiconductor nanostructures: fundamentals and recent advances. Springer Science & Business Media, 2006.

[88] Marco Fanciulli. Electron spin resonance and related phenomena in low-dimensional structures, volume 115. Springer Science & Business Media, 2009.

[89] G Kalosakas. Charge transport in dna: Dependence of diffusion coefficient on temperature and electron-phonon coupling constant. Physical Review E, 84(5):051905, 2011.

[90] Juan Daniel Torres, Raúl Hidalgo-Sacoto, Solmar Varela, and Ernesto Medina. Mechanically modulated spin-orbit couplings in oligopeptides. Physical Review B, 102(3):035426, 2020.

List of Figures

1.1 On the left, structure of the B-form DNA: a right handed double helix with ten nucleotides per turn (represented by colors as described in the top square). The chains are aligned in antiparallel orientations, where one chain goes from the $3'$ to the $5'$ sugar carbon and the other chain is reversed. In the right bottom square, a close-up of the structure can be seen. Bases are separated by a 3.4 Å translation along the helix axis. The phosphate group, the sugar and the base are represented as P, S and B respectively. The $3'$ and $5'$ sugar carbons are also represented[13]. 3

1.2 Experimental setup for the observation of spin polarization through DNA. The double stranded DNA was self-assembled on the gold crystal surface (golden balls). A linear polarized light (red arrows) passes unaffected by DNA and ejects unpolarized electrons (green arrows) from the gold substrate (left panel). Most electrons are spin filtered when passing trough the monolayer of DNA. Transmitted electrons are polarized with their spin aligned antiparallel to their velocity. Reflected electrons tunnel back to the substrate (right panel). Adapted from[32]. 5

1.3 Translational and rotational symmetries of DNA bases in π stack geometry. a) DNA base pair degrees of freedom including shear, buckle, stretch, propeller twist, stagger and opening movements. b) DNA steps degrees of freedom including slide, roll, twist, rise, shift and tilt movements. Adapted from [55]. 6

2.1 Example of the two center approximation for p_z orbitals. The bonding between these orbitals is considered to be a combination of a π-bond and a σ-bond, where the "amount" of each bonding is determined by the connecting vector $\hat{R}$. The angle between this vector and the vertical axis is β, and the angle between the Y axis and the projection of $\hat{R}$ onto the horizontal plane is α. 12

2.2 Structure of the double helix DNA from Varela et al. considered in the determination of the TB Hamiltonian with intrinsic spin-orbit coupling. Here, the orbital orientation is shown and each orbital is distinguished by colors: p_x is blue, p_y is red and p_z is green. Black dots represent other sites with orbitals. Parameters a and b are the radius and pitch of the helix respectively, and $\Delta\phi$ is the angle between bases. There are two set of axis: one is the fix basis $\{X,Y,Z\}$ and the other is the rotating basis $\{X,y,z\}$. Adapted from[81]. 13

2.3 Electron movement with the intrinsic SO effect. The electron at a p_z orbital moves to either a p_x or p_y orbital in the same site while changing its spin, then moves to another site into the p_z orbital with no spin change. Overall, the electron moves from one p_z orbital to another with the intra-helix coupling parameter V^{in}. The movement to the p_x orbital is not drawn to improve recognition of the electron transitions. 13
2.4 a) Here, the i and j orbitals are represented on $\mathbf{n}_i$ and $\mathbf{n}_j$ unit directions. These directions are independent on each other and their joining vector, $\mathbf{R}_{ji}$. The unit vectors, $\mathbf{n}_{i,j}$, are divided in parallel components with $\mathbf{R}_{ji}$, $\mathbf{n}(\phi_i)^{\parallel}$ and $\mathbf{n}(\phi_j)^{\parallel}$, and perpendiculars, $\mathbf{n}(\phi_i)^{\perp}$ an $\mathbf{n}(\phi_j)^{\perp}$. Then the σ bonding, which is produced when the orbitals follow the parallel direction, is the combination of $\mathbf{n}(\phi_i)^{\parallel}$ and $\mathbf{n}(\phi_j)^{\parallel}$ components; and the π bonding is the combination of the perpendicularly aligned orbitals. b) Description of the unit directions of p_x, p_y and p_z orbitals in the XY plane. These are divided in their fix basis components to be used in the calculation of SK parameters. The p_z is completely in $\hat{Z}$ while p_x and p_y have components in $\hat{X}$ and $\hat{Y}$ directions. 15

3.1 Structure of the double helix model of DNA in the fixed basis $\{X,Y,Z\}$. a) Side view with intra-helix, $\tau_{1,2}^{A,B}$, and inter-helix, τ_3, base vectors and pitch, b. b) Top view of a helix with rotation angle between two intra-helix bases, $\Delta\phi$, and radius, a. c) 3D view with chiral angle, η, and rotating system basis vectors $\{x,y,z\}$. Adapted from[62]. 18
3.2 A detailed view of the unit vectors connecting the sites in the structure model of DNA with the fix basis axis. From this image, the 3 connecting vectors can be deduced and these are defined in Eq. 3.1 in the rotating basis. The amount of bases per turn in the model is actually 10 not 6; this was drawn to ease the identification of b as the pitch. The component in $\hat{y}$ of τ_1 the arc resulting from the radius, a, multiplied by the angle between sites, $\Delta\phi$. The component in $\hat{z}$ of τ_1 is the pitch, b, multiplied by the angle between each site, $\Delta\phi$, divided by 2π. τ_3 has only a component in $\hat{x}$ which is $-2a$. 19
3.3 Graphical description of the electron-phonon model. There are three couplings to first neighbors with each one corresponding to a translation of each base vector with an associated amplitude. The intra-helix couplings have amplitudes t^{in} and inter-helix has t^{out}. 20
3.4 Graphical description of the addition of the intrinsic SO effect. There are two additional couplings to first neighbors with each one corresponding to a translation of each intra-helix base vector with an associated amplitude V^{in}. 27